NDP
National Development Plan 2007 - 2013

epa
Environmental Protection Agency
An Ghníomhaireacht um Chaomhnú Comhshaoil

STRIVE
Report Series No.33

The Use of Mesoporous Silicas to Absorb and Separate Metals and Nanoparticles from Aqueous or Organic Solutions

STRIVE

Environmental Protection Agency Programme

2007-2013

SSTI
Strategy for Science, Technology and Innovation

Comhshaol, Oidhreacht agus Rialtas Áitiúil
Environment, Heritage and Local Government

Environmental Protection Agency

The Environmental Protection Agency (EPA) is a statutory body responsible for protecting the environment in Ireland. We regulate and police activities that might otherwise cause pollution. We ensure there is solid information on environmental trends so that necessary actions are taken. Our priorities are protecting the Irish environment and ensuring that development is sustainable.

The EPA is an independent public body established in July 1993 under the Environmental Protection Agency Act, 1992. Its sponsor in Government is the Department of the Environment, Heritage and Local Government.

OUR RESPONSIBILITIES

LICENSING

We license the following to ensure that their emissions do not endanger human health or harm the environment:

- waste facilities (e.g., landfills, incinerators, waste transfer stations);
- large scale industrial activities (e.g., pharmaceutical manufacturing, cement manufacturing, power plants);
- intensive agriculture;
- the contained use and controlled release of Genetically Modified Organisms (GMOs);
- large petrol storage facilities.
- Waste water discharges

NATIONAL ENVIRONMENTAL ENFORCEMENT

- Conducting over 2,000 audits and inspections of EPA licensed facilities every year.
- Overseeing local authorities' environmental protection responsibilities in the areas of - air, noise, waste, waste-water and water quality.
- Working with local authorities and the Gardaí to stamp out illegal waste activity by co-ordinating a national enforcement network, targeting offenders, conducting investigations and overseeing remediation.
- Prosecuting those who flout environmental law and damage the environment as a result of their actions.

MONITORING, ANALYSING AND REPORTING ON THE ENVIRONMENT

- Monitoring air quality and the quality of rivers, lakes, tidal waters and ground waters; measuring water levels and river flows.
- Independent reporting to inform decision making by national and local government.

REGULATING IRELAND'S GREENHOUSE GAS EMISSIONS

- Quantifying Ireland's emissions of greenhouse gases in the context of our Kyoto commitments.
- Implementing the Emissions Trading Directive, involving over 100 companies who are major generators of carbon dioxide in Ireland.

ENVIRONMENTAL RESEARCH AND DEVELOPMENT

- Co-ordinating research on environmental issues (including air and water quality, climate change, biodiversity, environmental technologies).

STRATEGIC ENVIRONMENTAL ASSESSMENT

- Assessing the impact of plans and programmes on the Irish environment (such as waste management and development plans).

ENVIRONMENTAL PLANNING, EDUCATION AND GUIDANCE

- Providing guidance to the public and to industry on various environmental topics (including licence applications, waste prevention and environmental regulations).
- Generating greater environmental awareness (through environmental television programmes and primary and secondary schools' resource packs).

PROACTIVE WASTE MANAGEMENT

- Promoting waste prevention and minimisation projects through the co-ordination of the National Waste Prevention Programme, including input into the implementation of Producer Responsibility Initiatives.
- Enforcing Regulations such as Waste Electrical and Electronic Equipment (WEEE) and Restriction of Hazardous Substances (RoHS) and substances that deplete the ozone layer.
- Developing a National Hazardous Waste Management Plan to prevent and manage hazardous waste.

MANAGEMENT AND STRUCTURE OF THE EPA

The organisation is managed by a full time Board, consisting of a Director General and four Directors.

The work of the EPA is carried out across four offices:

- Office of Climate, Licensing and Resource Use
- Office of Environmental Enforcement
- Office of Environmental Assessment
- Office of Communications and Corporate Services

The EPA is assisted by an Advisory Committee of twelve members who meet several times a year to discuss issues of concern and offer advice to the Board.

EPA STRIVE Programme 2007–2013

The Use of Mesoporous Silicas to Absorb and Separate Metals and Nanoparticles from Aqueous or Organic Solutions

(2005-ET-MS-30-M3)

STRIVE Report

Prepared for the Environmental Protection Agency

by

Department of Chemistry, University College Cork

Author:

Aoife M. Burke

ENVIRONMENTAL PROTECTION AGENCY

An Ghníomhaireacht um Chaomhnú Comhshaoil
PO Box 3000, Johnstown Castle, Co. Wexford, Ireland

Telephone: +353 53 916 0600 Fax: +353 53 916 0699
E-mail: info@epa.ie Website: www.epa.ie

ACKNOWLEDGEMENTS

This report is published as part of the Science, Technology, Research and Innovation for the Environment (STRIVE) Programme 2007–2013. The programme is financed by the Irish Government under the National Development Plan 2007–2013. It is administered on behalf of the Department of the Environment, Heritage and Local Government by the Environmental Protection Agency which has the statutory function of co-ordinating and promoting environmental research.

DISCLAIMER

The EPA STRIVE Programme addresses the need for research in Ireland to inform policymakers and other stakeholders on a range of questions in relation to environmental protection. These reports are intended as contributions to the necessary debate on the protection of the environment.

EPA STRIVE PROGRAMME 2007–2013

Published by the Environmental Protection Agency, Ireland

PRINTED ON RECYCLED PAPER

ISBN: 978-1-84095-315-2

Price: Free 08/09/150

Details of Project Partners

Aoife Burke
Lab343
Department of Chemistry
Kane Building
University College Cork
College Rd
Cork
Ireland

Tel.: +353 21 4902911
E-mail: Aoife.Burke@ucc.ie

David Healy
CRAIC Lab
Department of Chemistry
Kane Building
University College Cork
College Rd
Cork
Ireland

Tel.: +353 21 4903526
E-mail: d.healy@ucc.ie

John Hanrahan
Environmental Research Institute (ERI)
University College Cork
Lee Rd
Cork
Ireland

Tel.: +353 21 4901965
E-mail: j.hanrahn@glantreo.com

Justin Holmes
Department of Chemistry
Kane Building
University College Cork
College Rd
Cork
Ireland

Tel.: +353 21 4903608
E-mail: j.holmes@ucc.ie

Michael Morris
Department of Chemistry
Kane Building
University College Cork
College Rd
Cork
Ireland

Tel.: +353 21 4902180
E-mail: m.morris@ucc.ie

Table of Contents

Executive Summary

The conservation and protection of the environment is essential for the health of both humans and other organisms and, therefore, has increased the urgency for methods of removal of both metal ions and nanoparticles from the environment. Heavy metal ions are the most significant environmental pollutants found in waste water, thus raising concerns regarding the long-term effects of metal ion exposure on human health and natural ecosystems. The metal ions that cause most concern for human and animal health include chromium, nickel, manganese and iron, together with various heavy metals, due to their toxic properties when consumed in large quantities.

In 2004, the Irish Environmental Protection Agency (EPA) released guidelines for the tolerable limits of metallic ion concentration in drinking water supplies. These drinking water parameters incorporated guideline quantities for the following metal ions:

- Chromium at 50 µg/l
- Nickel at 20 µg/l
- Manganese at 50 µg/l, and
- Iron at 200 µg/l.

Industrial waste waters, especially mining and metallurgical waste waters, are believed to be the major sources of heavy metal ion contamination. The EPA also released strict guidelines for metal ion content within industrial waste water incorporating chromium at 0.5 mg/l and nickel at 0.5 mg/l. In 2004, the European Pollution Emission Register reported total metal ion emissions measured within 183 facilities around Ireland. These measurements included chromium at 152 kg and nickel at 221 kg. The evident difference between waste water metal content and the required drinking water metal content has led to a major focus on waste treatment and clean-up research to produce economic and effective methods for the removal of these metal ions.

The ability to remove metals from water can be greatly improved by technology developed at University College Cork (UCC) which uses a ‘smart’ material as a key part of the filtration system. This project explored the development of new nanostructured materials (silica) for effective treatment of various pollutants including metal ions and metal nanoparticles. Mesoporous materials are a relatively new material type that may have wide application as absorbents owing to their large surface areas, large pore volumes and large pore diameters. The ability to control the morphology and pore diameter of mesoporous silica opens up possibilities for commercial application as metal ion absorbents. Facile functionalisation of mesoporous silica spheres, with different chelating agents or ligands, allows specific metal ion pollutants to be targeted and removed from aqueous or organic systems.

Research completed in UCC included mesoporous silica spheres being synthesised and functionalised and subsequently used as absorbents for metal ions, both single metal and mixed metal solutions as well as metallic nanoparticles. Single metal ion extraction was carried out over the pH range between 4 and 10 to identify the optimum pH for removing each metal ion. Metal ion extractions were also carried out in non-buffered water to replicate the natural environmental conditions for these metal ions. The absorbents used for these extraction experiments consisted of mesoporous silicas functionalised with aminopropyl ligands (Si–NH), mesoporous silicas functionalised with a mercaptopropyl ligand (Si–SH) and mesoporous silicas functionalised with both aminopropyl and mercaptopropyl ligands (SH–Si–NH). Different metal ions form more stable complexes with either aminopropyl or mercaptopropyl ligands.

Maximum absorptive capacities of the mesoporous spheres for metal ions were determined to be:

- 384 µmol/g for chromium
- 340 µmol/g for nickel

- 358 µmol/g for iron
- 364 µmol/g for manganese, and
- 187 µmol/g for palladium.

The absorbents are also used to remove mixed metal ion solutions in non-buffered water and an environmental sample was supplied by the EPA to highlight the possibilities of using these materials for the clean-up of waste water streams. Further to these experiments, both the parent silica samples and the functionalised silica samples were tested for their ability to remove gold nanoparticles from solution. Maximum nanoparticle extraction could be approximated at 0.1203 M of gold nanoparticles per gram of silicon. These project results clearly demonstrate the potential of these absorbents to be applied as alternative filtration systems.

1 Introduction

1.1 Mesoporous Materials: Background

Mesoporous materials are defined by the International Union of Pure and Applied Chemistry (IUPAC) as porous substances with pore diameters between 2 and 50 nm (IUPAC, 1976). Since the discovery of Mobile Composition of Matter (MCM)-type materials by the Mobil Corporation in 1992, mesoporous silica has been the centre of much interest within the material science community (Ma *et al.*, 2003; Hanrahan *et al.*, 2004). This interest is fostered to some extent by their two-dimensional structures but also due to their expected applications in catalysis, sensing, molecular sieving, templating of nanostructures and in separation and absorption processes (Kim *et al.*, 2004). The advantages of using mesoporous materials in these areas include the ease of synthesis from commercially available reagents, high specific surface areas, controllable pore dimensions and high hydrothermal stability, which allow mesoporous materials (Beck *et al.*, 1992; Kresge *et al.*, 1992) to be employed in a number of commercial areas that include molecular and protein separations (Estermann *et al.*, 1991), catalysis (Selvam *et al.*, 2001; Linssen *et al.*, 2003), chromatography (Gallis *et al.*, 1999), and as templates for controlling the aspect ratio of quantum-confined nanoparticles and nanowires (Coleman *et al.*, 2001a,b,c; O'Neil *et al.*, 2002; Crowley *et al.*, 2003). In particular, mesoporous thin films have recently been utilised as templates for creating high-density arrays of semiconductor (Ryan *et al.*, 2003) and metallic (Fukuoka *et al.*, 2002) nanowires and carbon nanotubes (Wu and Bein, 1994), allowing the potential creation of multilayered microelectronic device architectures. Mesoporous silicas with large surface areas, ordered porosity and large pore diameter are also seen as promising candidates for absorption, host–guest encapsulation for advanced nanomaterials (Darbandi *et al.*, 2006), controlled release substances and as potential stationary phases for high-performance liquid chromatography (HPLC) (Healy *et al.*, 2003) and biological absorbents (Zhang *et al.*, 2007).

The synthesis of mesoporous materials relies on a supramolecular templating mechanism, in which the ordered aggregation of amphiphilic molecules (surfactants) functions as a structure-directing template for the condensation of an inorganic framework. The template is then removed through extraction and/or calcination processes, leaving the desired inorganic pore structure. A simple illustration of this process is shown in Fig. 1.1.

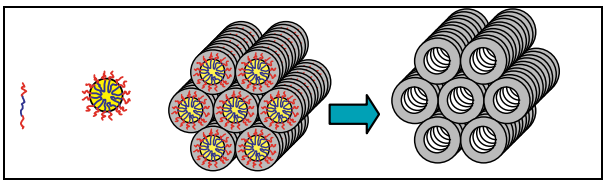

Figure 1.1. The schematic shows the process for synthesising mesoporous silica using surfactant, a silica source and acidic solution.

The pore structures developed in mesoporous materials are classified into three phases, namely hexagonal, cubic and lamellar as shown in Fig. 1.2. These phases are identified and categorised using X-ray diffraction (XRD) and transmission electron microscopy (TEM). The particular phase present after synthesis is dependent on the concentration of the surfactant being used, the nature of the surfactant (length of hydrophobic and hydrophilic chains) and reaction parameters (temperature and pH) (Zhao *et a*l., 1996).

Particular surfactants are used to template particular mesoporous materials and can be categorised based on their net charge into anionic (negative charge), cationic (positive charge) and non-ionic (neutral charge). Non-ionic surfactants were used throughout this study and are further classified as amphiphilic copolymers consisting of poly(propylene oxide) (PPO) and poly(ethylene oxide) (PEO) blocks, in particular triblock copolymers consisting of PEO–PPO–PEO blocks were used. A PPO polymer phase separates

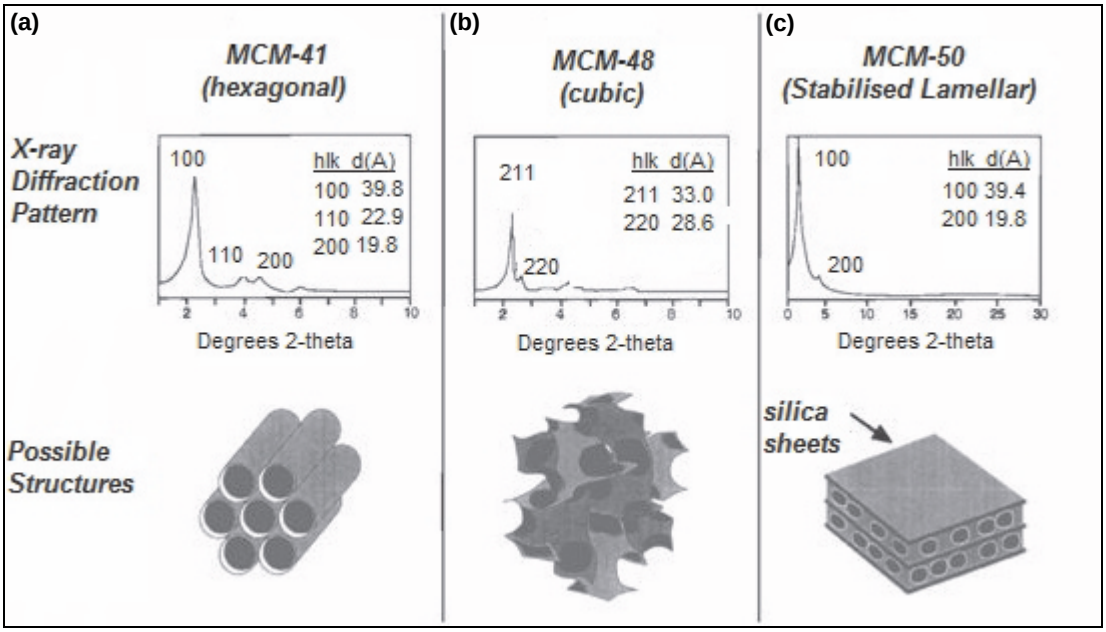

Figure 1.2. Proposed structures of (a) hexagonal, (b) cubic, and (c) lamellar mesoporous silica with accompanying X-ray diffraction structures (Copley, 2006).

from water at a relatively low temperature of 5°C, while PEO has high solubility in water (Kipkemboi *et al.*, 2001). Block copolymers consist of a central PPO block surrounded by two PEO blocks giving a hydrophobic core with a hydrophilic coating. This block copolymer structure causes the hydrophilic centres of the copolymer molecules to agglomerate when saturated in an aqueous acidic solution; during synthesis these result in the formation of surfactant micelles, shown in Fig. 1.1. Altering the molecular weight and the molar ratio of PPO to PEO alters the amphiphilic nature of the block copolymer. For hexagonal mesoporous materials templated from PEO–PPO–-PEO triblock surfactants, the wall thickness is largely dependent on the length of the PEO blocks, while the PPO block length has a great effect on the pore diameter. The PPO block length also influences the templating ability – longer PPO blocks result in highly ordered domains (Flodstrom and Alfresson, 2003). This enables block copolymers to be refined for specific applications.

Reaction temperature is a critical variable during the synthesis of mesoporous materials. With a typical block copolymer structure of PEO_x–PPO_y–PEO_x (where x = 20–100 and y = 20–100), the PEO blocks become less soluble in water as the temperature rises, causing the molecule to become more hydrophobic. The increased hydrophobicity of the molecule in turn causes an increase in the pore size of the templated mesoporous material. This behaviour is due to the stereochemistry attached to the PEO group which at the higher temperature/energy adopts the anti-conformation which has no dipole moment, in sequence increasing hydrophobic behaviour.

The BASF Corporation supplies many triblock copolymers under the trade name Pluronics®. These include P123 and F127, both of which have $PEO_xPPO_yPEO_x$ structures – $PEO_{20}PPO_{70}PEO_{20}$ and $PEO_{106}PPO_{70}PEO_{106}$, respectively. These surfactants can be used independently, or mixed together, to produce specific molecular structures and can be controlled by temperature to produce the required phase and pore size of a specific mesoporous material. Control of the reaction conditions can also produce mesoporous silica particles with varying morphology, e.g. spheres, nanoparticles, rods, as opposed to powders. The different structures that can be produced may have several commercial advantages, e.g. spheres are extensively utilised in chromatography columns to obtain optimum flow characteristics of the effluents.

The application of mesoporous silica spheres as absorbent materials is well established in academic research. For example, the sorption of mercury ions using mesoporous silica as a base material has been reported by Fryxell *et al.* (1997) and Mercier and Pinnavaia (1998). Copper, zinc, nickel and cadmium metal ions have also been extracted using mesoporous silica (Bois *et al.*, 2002; Northcott *et al.,* 2006). Silica has also been applied as a detection material for mycotoxins and is used as a stationary phase in HPLC (coupled with fluorescence detection) (Jaimez *et al.*, 2000; Avantaggiato *et al.*, 2004).

1.2 Chemical Modification of Mesoporous Silica Surfaces for Absorption Applications

As outlined above, the properties of mesoporous silica make it an excellent support material for many applications, such as an absorptive material for metal ions, nanoparticles and mycotoxins from the environment. However, for each of these applications the parent mesoporous silica requires chemical surface alteration to fulfil the different absorptive requirements.

The surface alteration of the parent mesoporous silica is completed using similar experimental procedures irrelevant of the category of ligand used for functionalisation. A number of methods, described above in Section 1.1, can be utilised to produce mesoporous silica particles with large pore diameters. These large mesopores allow attachment of bulky ligands, e.g. triamines, within the channels of the silica while reducing pore blockage of the material, thus keeping the pores available for absorption applications. The number of silanol groups (as shown in Fig. 1.3) is an important variable to consider when functionalising the mesopores in silica as bonding of the ligand usually occurs at functional hydroxyl groups. The greater the number of silanol groups on the walls of the porous channels, the higher the loading of ligand that can be bonded to the silica. Unmodified mesoporous silica samples contain silanol groups on the surface of the materials and also within the porous channels. These silanol groups (known as free silanol groups) typically release hydrogen upon

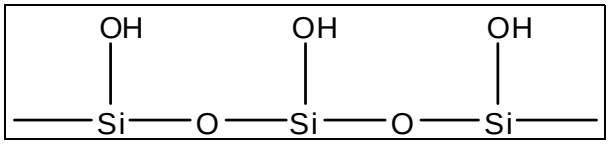

Figure 1.3. Schematic of the surface silanol groups present on mesoporous silica.

functionalisation, allowing attachment of the ligand to the silica surface.

There are four different bonds used to functionalise silica with particular ligands: Si–O–C linkage, Si–N linkage, Si–C linkage and Si–O–Si–R linkage. Within this report the Si–O–Si–R and Si–O–C linkages are mostly used, illustrated in Fig. 1.4.

$$RSi - X + Si - OH \rightarrow RSi - O - Si + XH$$

$$RC - X + Si - OH \rightarrow RC - O - Si + XH$$

Figure 1.4. Chemical representation of functionalising procedure showing attachment to the silica through release of the hydrogen.

Here, *X* is a methyl group (hydrophobic alkyl functional group) or a methoxy group (a functional group consisting of a methyl group and oxygen). These groups then react with the free silanol groups to achieve ligand attachment. When the methyl group of the ligand reacts with the silanol group, methane is released, whereas when the methoxy group reacts with the free silanol group, methanol is released. The symbol *R* refers to the functional group within the ligand, specifically chloro, alkoxy, aminopropyl and mercaptopropyl groups. These functional groups dictate the absorption application of each ligand.

Generally, there are two types of functionalisation phases: monomeric and polymeric. The water content within the functionalising reaction dictates the nature of the bonding phase. Monomeric phases are produced by the reaction of ligands in the absence of water. The structure of the monomeric phase contains the ligands in a vertical morphology as shown in Fig. 1.5. Functionalising the mesoporous silica in the absence

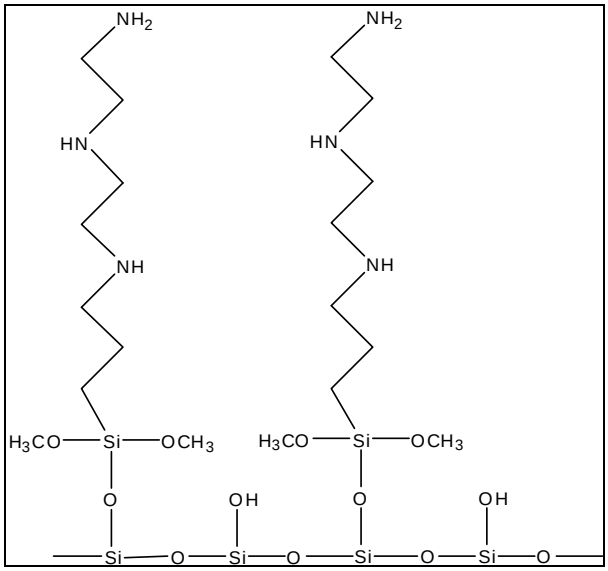

Figure 1.5. Monomeric phase showing vertical functionalising in the absence of water.

of water requires the removal of the silanol groups from the surface of the mesoporous silica material. In doing so, the ligand then penetrates into the channels of the mesoporous sphere giving a more predictable and orderly material. Also, this material can show higher absorption efficiency for smaller molecules.

The polymeric phase involves the reaction of the functional groups in the presence of water and is a cross-linked phase which is not restricted to one layer. The ligand polymerises vertically but is not as ordered as the monomeric phase as shown in Fig. 1.6. When water is present during the functionalising process the free silanol groups are still present causing the ligands to attach on the surface of the mesoporous material. The advantage of this functionalising is that it allows absorption of larger molecules to the surface of the mesoporous material.

A number of ligands have been bonded to silica each one allowing different ions and molecules to be absorbed. For example, functionalisation of mesoporous silica with a mercaptopropyl ligand for mercury extraction has been demonstrated by both Fryxell *et al.* (1997) and Mercier *et al.* (1998). Chloro ligands have been applied for extraction of copper and zinc (Northcott et al., 2006). Bois *et al.* report sorption of copper, nickel and cadmium using aminopropyl or mercaptopropyl ligands (Bois *et al.*, 2002). In this

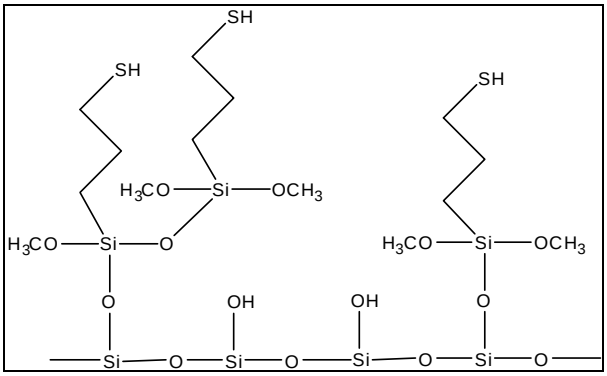

Figure 1.6. Polymeric phase functionalising in the presence of water.

study, different ligands were attached to the mesoporous silica using both monomeric and polymeric phases and each ligand was examined for its extraction efficiency of different molecules.

1.3 Mesoporous Silica in Metal Ion Remediation Applications

Heavy metal ions are the most significant environmental pollutants found in waste water, thus raising concerns regarding the long-term effects of metal ion exposure on human health and natural ecosystems (Celik and Demirba, 2005; Say *et al.*, 2006). The metal ions that cause most concern for human and animal health include chromium, nickel, manganese and iron, together with various heavy metals, due to their toxic properties when consumed in large quantities (Ajay *et al.*, 2005; Celik and Demirba, 2005). In 2004, the Irish EPA released guidelines for the tolerable limits of metallic ion concentration in drinking-water supplies. These drinking-water parameters incorporated guideline quantities for the following metal ions: chromium at 50 µg/l, nickel at 20 µg/l, manganese at 50 µg/l and iron at 200 µg/l. Industrial waste waters, especially mining and metallurgical waste waters (Ekmekyapara *et al.*, 2006), are believed to be the major sources of heavy metal ion contamination. The Irish EPA also released strict guidelines for metal ion content within industrial waste water, incorporating chromium at 0.5 mg/l and nickel at 0.5 mg/l (EPA, 2006). In 2004, the European Pollution Emission Register (EPER) reported total metal ion emissions measured within 183 facilities around Ireland. These measurements included chromium at

152 kg and nickel at 221 kg. The evident difference between waste-water metal content and the required drinking-water metal content has led to a major focus on waste treatment and clean-up research to produce economic and effective methods for the removal of these metal ions. Table 1.1 shows a list of the major industries employing and releasing different heavy metals into the environment.

The increasing pollution problem within the environment has now reached a level of potential danger to the entire population. This continuous deterioration is due to environmental pollutants released through industrialisation, domestic activities, atomic explosions and other environmental changes (Ali and Aboul-Enein, 2006). Pollutants within the environment refer to any undesirable or toxic chemical, organism or object present in the environment. These pollutants can come from many different sources and enter the air, water and land in a variety of ways. The presence of these toxic pollutants is very harmful to humans and other important organisms. In general, environmental pollutants can be categorised into two classes: chemical and biological. Chemical pollution refers to both organic and inorganic compounds, the most serious of which are inorganic compounds, particularly when in the form of toxic metal ions as these can often be carcinogenic (Nriagu, 1989; Hempel *et al.*, 1995; Carro and Mejuto, 2000; Ali and Aboul-Enein, 2006). Metal ions occur within the environment in many different oxidation states forming various species. The toxicity of a metal ion can depend on its oxidation state, as one oxidation state can be more toxic than others (Stoeppler, 1992). This report is mainly concerned with toxic metal ion and metal nanoparticle pollutants present within the hydrosphere of the environment, consisting of all waterbodies including ocean, surface and groundwater. In this study, a sample of these pollutants are removed from solution using the mesoporous material previously discussed. The principle route of toxic metal ions into the human body is through waterbodies and foodstuffs, therefore increasing the necessity to monitor and remove metal ions from drinking-water sources.

Low concentrations of some metal ions are essential for human, animal and plant development but these metal ions can become toxic and result in diseases when ingested at higher concentrations. When metal ions are ingested they are absorbed through the gastrointestinal tract into the bloodstream, leading to an increase in concentration of the metal ion with continuous exposure, even at low concentrations. Metal ions disturb many enzymatic functions in biological systems. These hazardous metal ions enter the drinking-water supply when groundwater and surface water become contaminated. Water supplies become contaminated when oxidation of mineral

Table 1.1. Major industries employing and releasing heavy metals as reported in Ali and Aboul-Enein, 2006.

Industries	Cadmium	Chromium	Copper	Iron	Manganese	Lead	Zinc
Paper mill		X	X			X	X
Petrochemicals	X	X		X		X	X
Fertilisers	X	X	X	X	X	X	X
Petroleum refining	X	X	X	X		X	X
Steelworks	X	X	X	X		X	X
Non-ferrous metalworks	X	X	X			X	X
Aircraft plating	X	X	X			X	
Cement		X					
Textiles		X					
Leather tanning		X					
Steam generation		X					X

species within water cause metal ions to become soluble and enter the environment through the drainage system (Ali and Aboul-Enein, 2006). Water is the main component of the ecosystem and is also the most contaminated, therefore it needs more focus for clean-up procedures.

Many studies have been completed to identify the effects of metal ions on humans. Iron, copper, chromium and vanadium have been shown to undergo redox cycling, whereas cadmium, mercury and nickel reduce glutathione and protein-bound sulfhydryl groups. These changes are responsible for the production of reactive oxygen species such as superoxide ions and hydrogen peroxide, resulting in enhanced lipid peroxidation, DNA damage and altered calcium and sulfhydryl homeostasis (Stohs and Bagchi, 1995). Other studies also suggest that metal ions increase the production of tumour necrosis factor alpha which activates kinase C and produces stress proteins (Ali and Aboul-Enein, 2006). Mechanisms associated with the toxicities of metal ions are similar to mechanisms produced by organic xenobiotics.

Hexavalent chromium or Cr(VI) is recognised as a human carcinogen (IARC, 1999). Many different industries work with hexavalent chromium, exposing workers to this metal ion which acts as a sensitiser and irritant when in contact with the skin. Once hexavalent chromium has entered an organism it reduces its oxidation state, firstly to metastable pentavalent chromium, then to trivalent chromium, which in turn binds to proteins creating haptens causing an immune system reaction. Pentavalent chromium is identified as the main carcinogenic species. During reoxidation of pentavalent chromium, by hydrogen peroxide molecules present in cells, hydroxyl radicals are produced causing damage to the cells (IARC, 1999). Once chrome sensitivity has developed it becomes very persistent causing dermatitis even when in contact with chromate-dyed textiles.

Iron is an essential component required by nearly all organisms. In cells, iron is generally stored within the cell in the metalloproteins. When iron does not specifically bind to cellular components it causes catalytic production of toxic free radicals. These free radicals are highly reactive and can cause damage to DNA, protein, lipids and other cellular components. Iron distribution needs to be regulated due to its high potential for biological toxicity; a bacterium requires iron so these regulations limit the availability of iron to bacteria. High blood concentrations of iron (exceeding the recommended 20 mg/kg) cause damage to the heart and liver, leading to serious long-term organ problems.

Many different nickel compounds are known to be carcinogenic including nickel sulfide (Dunnick *et al.*, 1995; Kasprzak *et al.*, 2003). Nickel compound exposure should not exceed 0.05 mg/cm^3 in nickel equivalents per 40-h working week. The EU has regulated the quantity of nickel within products which come in contact with human skin as sensitised individuals can show an allergic reaction to nickel (Nestle *et al.*, 2002).

Although manganese compounds are less toxic than iron, nickel and copper, they can be toxic in excessive amounts. Manganese exposure has also been linked to impaired motor skills, cognitive disorders and neurodegeneration (Yang *et al.*, 2005).

Cadmium and cadmium compounds have been identified as carcinogens and can induce many types of cancer (NTP, 2008). Research shows that cadmium becomes toxic to humans when carried into the body bound to zinc-binding proteins. Zinc and cadmium contain common oxidation states and ionise to become similar sizes. Due to this similarity, cadmium can replace zinc in biological systems. The strong bond that cadmium makes with these biological systems makes it notoriously difficult to remove. The primary exposure source of cadmium is through inhalation, resulting in pneumonitis and pulmonary oedema (Hayes and Holland, 2001). There have been toxicity recordings as a result of long-term exposure to cadmium in contaminated food and water, leading to itai-itai disease and renal abnormalities (Nogawa, 2004).

Like most metal ions, copper is an essential nutrient for plants and animals and can be found in the bloodstream; however, in excessive amounts it can be poisonous and even fatal to organisms. All copper compounds, especially when exceeding 30 g of copper sulfate, are considered toxic and lethal to humans. The

suggested safe level of copper in drinking water for humans is reported to be between 1.5 and 2 mg/l. When copper is excessive it becomes toxic and can inhibit enzyme dihydrophil hydratase, an enzyme involved in haemopoiesis. Water containing too much copper has also been reported to damage marine life, including damage to gills, liver, kidneys and the nervous system of fish and other creatures.

Lead is known to be one of the most toxic metal ions when humans are exposed to it. Lead poisoning is a medical condition causing irreversible neurological damage as well as renal disease, cardiovascular effects and reproductive toxicity. There are guidelines for lead exposure but the threshold for lead blood levels is still unknown (Esmat, 1993). Lead toxicity comes from its ability to mimic other biologically important metals, for example calcium, iron and zinc. It can mimic these metal ions by binding and interacting with the same proteins and molecules but cannot carry out the same reactions, such as producing enzymes necessary for certain biological processes.

The Irish EPA has drinking-water standards with two levels of protection. The aim is to have a lead level of zero, a level considered safe by toxicological and biomedical considerations, but the EPA has established a level of 10 µg/l. The EPA drinking-water regulations of several metal ions are shown in Table 1.2 (EPA, 2004).

Table 1.2. EPA drinking-water regulation parameters (Ireland).

Metal	Parameter
Chromium	50 µg/l
Nickel	20 µg/l
Cadmium	5 µg/l
Copper	2 mg/l
Lead	10 µg/l
Mercury	1 µg/l

1.4 Mesoporous Silica in Nanoparticle Remediation Applications

Nanoparticles are defined as entities with one or more dimensions of the order of 100 nm or less (EPA, 2007). They can be found in spherical, tubular or irregular shapes and can exist in fused, aggregated or agglomerated structures. Nanoparticles can be further categorised into natural and anthropogenic nanoparticles which subsequently can be defined by their chemical composition: either carbon-containing or inorganic nanoparticles. Naturally occurring nanoparticles, either carbon-containing or inorganic, can be divided into biogenic, geogenic, atmospheric and pyrogenic. Soot is an example of a naturally occurring geogenic nanoparticle, produced by incomplete combustion of fossil fuels and vegetation and can have particle sizes that fall partially within the nanoscale domain (Nowack and Bucheli, 2007). Additional examples are given in Table 1.3. Both carbon-containing and inorganic anthropogenic nanoparticles are defined as either the by-product of a process or intentionally engineered nanoparticles, also shown in Table 1.3. Recently the anthropogenic production of nanoparticles has increased due to the ability to synthesise and manipulate these materials for application in electronic, biomedical, pharmaceutical, cosmetic, environmental, catalytic and material applications.

The current use and production of nanoparticles is difficult to define but an estimate for the production of engineered nanomaterials was reported as 1,000 t in 2004, with an expected increase to 58,000 t between 2011 and 2020 (Maynard, 2006). Currently in industry, silica, alumina and ceria nanoparticles are used in chemical–mechanical polishing of silica wafers (Murray, 2004); ceria nanoparticles are also used for hydrocarbon combustion in turbine engines and fuel cells (Madler *et al.*, 2002; Hu *et al.*, 2007), and zinc and titanium oxide nanoparticles are produced for use as UV absorbers and sunscreen (Becheri *et al.*, 2008). A comprehensive list of nanoparticle applications is given in Table 1.4.

This significant increase in nanoparticle production will in turn increase human exposure to nanoparticles, causing increased scrutiny and concern for the effects of nanoparticles on the environment. The mobility, bioavailability and toxicity of nanoparticles need to be assessed and understood to properly quantify the risks associated with them. The exposure pathways for

Table 1.3. Classification and examples of nanoparticles.

Nanoparticle classification	Formation	Examples
Natural		
Carbon-containing	Biogenic	Organic colloids
	Geogenic	Soot
	Atmospheric	Aerosols
	Pyrogenic	Soot
Inorganic	Biogenic	Metals
	Geogenic	Oxides
	Atmospheric	Aerosols
Anthropogenic		
Carbon-containing	By-product	Combustion
	Engineered	Polymeric nanoparticle
Inorganic	By-product	Combustion
	Engineered	Metals

nanoparticles are key to evaluating this increasing risk as shown in Fig. 1.7.

There are two categories of concern when referring to the release of nanoparticles: point sources and non-point sources. Point sources include direct release from production facilities, landfills or waste-water treatment plants, whereas non-point sources refer to release due to the wear from materials containing nanoparticles. When nanoparticles are released, whether directly or indirectly, they finish up in water or soil through sewage treatment plants, waste handling or aerial deposition, leading to human exposure.

Nanoparticles entering the body can become coated with proteins, leading to severe effects on the protein function and conformation. Concentrations of certain proteins increase on the particle surface perhaps resulting in attenuation or amplification of activity, protein aggregation and disruptions of the protein. Due to the protein absorption onto the nanoparticle there is the risk of an immune response or protein misfolding diseases (Lundqvist *et al.*, 2004, 2005; Lindman *et al.*, 2006; Roach *et al.*, 2006). Evidence shows that nanoparticles can be absorbed by a variety of mammalian cell types and are able to cross the cell membrane and enter the system (Lyon *et al.*, 2006; Rothen-Rutishauser *et al.*, 2006; Smart *et al.*, 2006). This uptake is dependent on the size of the nanoparticles and occurs *via* endocytosis or phagocytosis in specialised cells. The cells store the nanoparticles within either the vesicles or the mitochondria, causing a toxic response. On an organism level, the toxicity occurring is evident through inflammation and fibrosis, whereas oxidative stress, antioxidant activity and cytotoxicity are monitored on the cellular level, leading to respiratory and cardiovascular diseases in humans (Oberdorster *et al.*, 2004). Figure 1.8 shows TEM results of human aortic endothelial cells during direct exposure to metal oxide nanoparticles.

Exposure pathways of nanoparticles vary depending on the handling procedure in the workplace, how the nanoparticles separate within various media such as air and water, the mobility of the nanoparticles in each of these solvents, and the magnitude of their sources. Although much research is currently being completed on the toxicity of nanoparticles, there are insufficient data to allow a realistic risk assessment of nanoparticles within the environment. Currently, regulation on the dosage of particles is defined by mass per unit volume, which does not take into

Table 1.4. Nanoparticle properties and applications within industry (after Malvern, 2007).

Property	Application
Optical	• Anti-reflection coatings • Tailored refractive index of surfaces • Light-based sensors for cancer diagnosis
Magnetic	• Increased density storage media • Nanomagnetic particles to create improved detail and contrast in magnetic resonance images
Thermal	• Enhance heat transfer from solar collectors to storage tanks • Improve efficiency of coolants in transformers
Mechanical	• Improved wear resistance • New anti-corrosion properties • New stronger and lighter structural materials and composites
Electronic	• High-performance and smaller components, e.g. capacitors for small consumer devices such as mobile phones • Displays that are cheaper, larger, brighter, and more efficient • High-conductivity materials
Energy	• High-energy density and more durable batteries • Hydrogen storage applications using metal nanoclusters • Electrocatalysts for high-efficiency fuel cells • Renewable energy, ultra-high-performance solar cells • Catalysts for combustion engines to improve efficiency, hence economy
Biomedical	• Antibacterial silver coatings on wound dressings • Sensors for disease detection (quantum dots) • Programmed release drug-delivery systems • ‘Interactive’ food and beverages that change colour, flavour or nutrients depending on a diner’s taste or health
Environmental	• Clean-up of soil contamination and pollution, e.g. oil • Biodegradable polymers • Aids for germination • Treatment of industrial emissions • More efficient and effective water filtration
Surfaces	• Dissolution rates of materials are highly size dependent • Activity of catalysts • Coatings for self-cleaning surfaces, e.g. Pilkington’s glass
Personal care	• Effective clear inorganic sunscreens

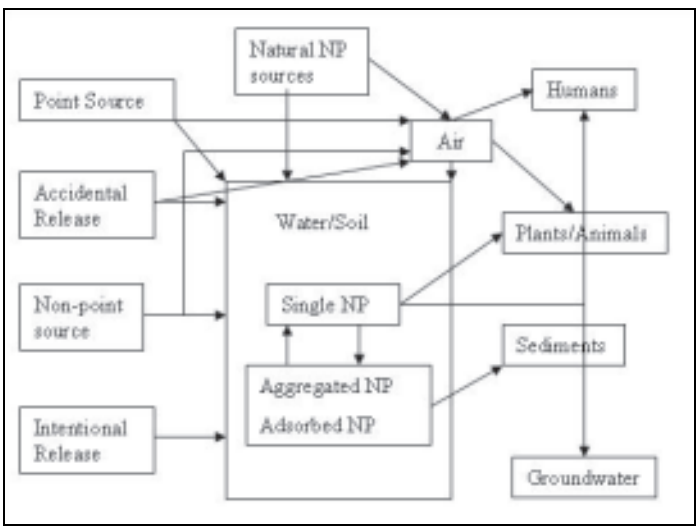

Figure 1.7. Nanoparticle (NP) pathways from the anthroposphere into the environment, reactions in the environment and exposure of humans (after Nowack and Bucheli, 2007).

account particle size, agglomeration and surface reactivity. The risk assessment will become more relevant in the near future with the increase of nanomaterial production. With these possible risks in mind, nanoparticle clean-up from industrial waste water also needs assessment and study. In this study mesoporous silica spheres, unfunctionalised and functionalised with aminopropyl and mercaptopropyl ligands, are utilised as an absorbent for gold nanoparticles from solutions.

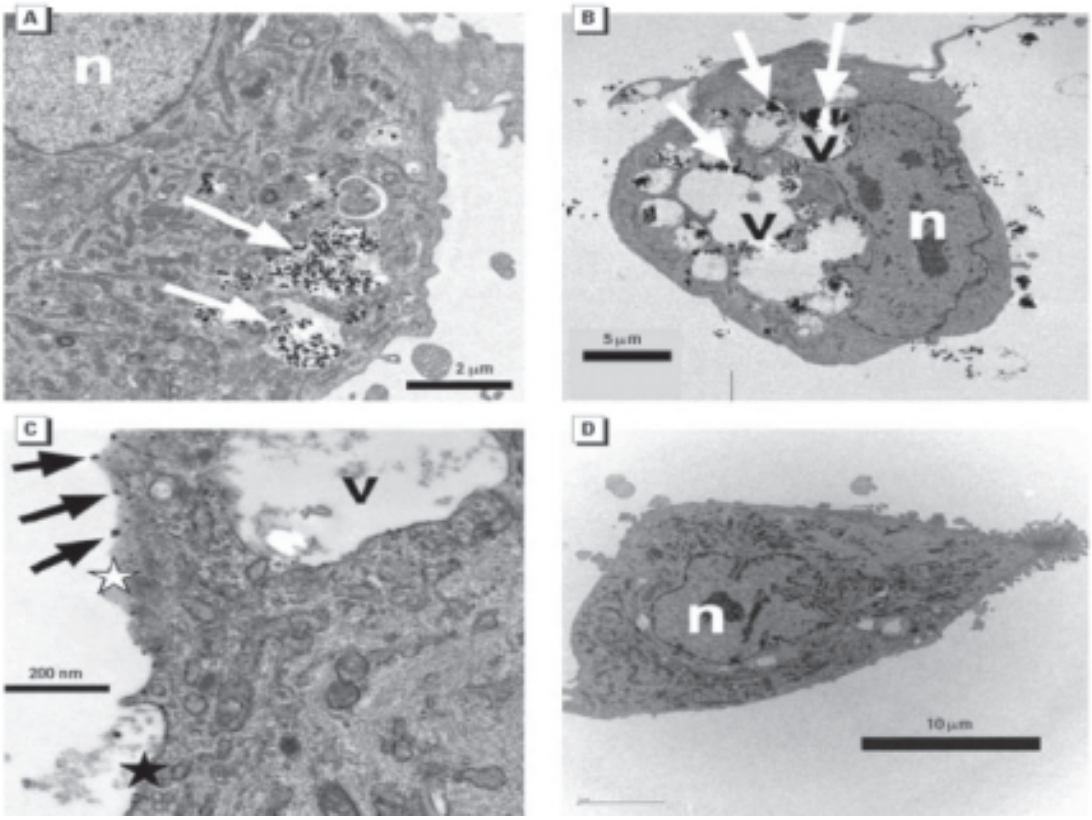

Figure 1.8. Thin-section transmission electron microscopy images incubated with metal oxide nanoparticles (A) iron oxide (Fe_2O_2), (B) yttrium oxide (Y_2O_2), (C) zinc oxide (ZnO), and (D) the control sample (reproduced from Gojova *et al.* (2007) with permission from *Environmental Health Perspectives*).

2 Experimental

2.1 Synthesis of Mesoporous Silica Spheres

Mesoporous silica spheres were synthesised using the triblock copolymer surfactants P123 ($PEO_{20}PPO_{69}PEO_{20}$) and F127 ($PEO_{106}PPO_{70}PEO_{106}$), supplied by BASF, UK, as supramolecular templates similar to a method reported by Kim *et al.* (2004). The ageing time and temperature of the synthesis procedure were altered to find the optimum parameters to produce large-pore mesoporous silica spheres. A mixture of copolymers was used to refine the mesophase and define the spherical morphology of the mesoporous material. The quantity of copolymer, relative to the water content, was increased to further increase the pore size of the mesoporous silica spheres. The parameters of the synthesis procedure are outlined in Table 2.1.

Table 2.1. Synthesis parameters for generating large-pore mesoporous spheres.

Temperature	P123 content	F127 content	Ageing time
60°C	1 g	5.3 g	1–7 days
110°C	2 g	5.3 g	1–7 days

A mixture of F127 and P123 was dissolved in an aqueous solution of HCl (1.6 M, 280 ml). Tetraethoxysilane (TEOS), purchased from Fluka, Ireland, was then added to the solution and stirred (400 rev./min at 35°C for 15 min. The mixture was then allowed to age without stirring at 35°C for 24 h before being transferred in a sealed vessel to an oven, at either 60 or 110°C, for further ageing of between 1 and 7 days. The starting molar composition of the mixture was 0.0037 F127:0.0016 P123:1 TEOS:4.2 HCl:144 H_2O or 0.0037 F127:0.0032 P123:1 TEOS:4.2 HCl: 144 H_2O. The white precipitate product was filtered without washing and dried at 60°C, followed by filtration with ethanol. Subsequently, the product was calcined at 550°C for 5 h to ensure complete template removal.

2.2 Functionalisation of Mesoporous Silica Spheres

2.2.1 Mono-functionalising procedure in the absence of water

Calcined mesoporous silica solid was modified with the chosen ligand:

- *N*-3-trimethoxysilylpropyldiethylenetriamine, or
- 3-mercaptopropyl-trimethoxysilane

both purchased from Sigma–Aldrich, Ireland. A 1-g sample of the mesoporous silica material was dehydrated at 120°C under vacuum before being stirred in 100 ml of dry toluene, containing 5 ml of the ligand, under refluxing conditions for 5 h. After refluxing, samples were washed with dry toluene under vacuum and collected for analysis. Figure 2.1 shows a schematic representation of the functionalising process which is thought to occur *via* reaction at the surface hydroxyl sites.

2.2.2 Bi-functionalising procedure

One gram of dehydrated calcined mesoporous silica spheres was added to 100 ml of dry toluene, containing 5 ml of trimethoxysilylpropyldiethylenetriamine, and refluxed under nitrogen at 110°C for 6 h. The sample was then washed under vacuum using dry toluene. The sample was recovered and added to 100 ml of dry toluene, containing 5 ml of 3-mercaptopropyl-trimethoxysilane, and refluxed under nitrogen for a further 6 h. The final product was filter recovered and washed with dry toluene. Figure 2.2 shows a schematic representation of the bi-functionalising reaction process.

2.3 Metal Ion and Nanoparticle Extraction Experimental

2.3.1 Extraction procedure for single metal ions

Standard metal ion (nickel, chromium, palladium, iron and manganese, purchased from Aldrich) nitrates of 1,000 ppm were diluted to a 10 ppm solution in various solvents, including pH buffers at a pH of 4 (citric acid,

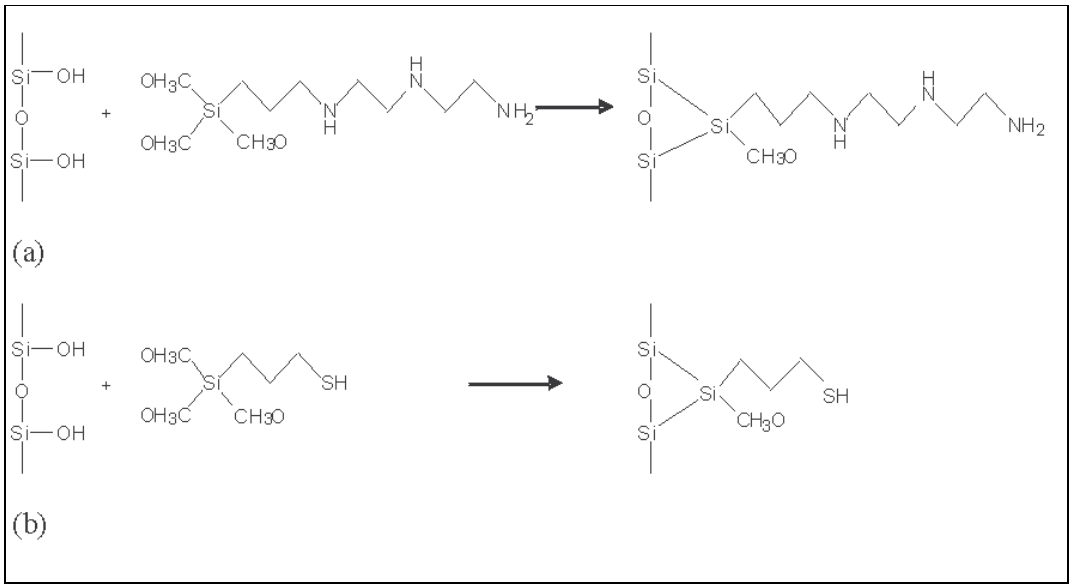

Figure 2.1. Schematic representation of the functionalising procedure (a) the aminopropyl group (–NH) and (b) the mercaptopropyl group (–SH).

sodium azide, sodium chloride and sodium hydroxide solution), a pH of 7 (potassium dihydrogen phosphate and sodium hydroxide solution) and a pH of 10 (borax and sodium hydroxide solution) and non-buffered water in an attempt to identify the optimum extraction conditions. Approximately 0.01 g of aminopropyl, mercaptopropyl or bi-functionalised mesoporous silica was added to 20 ml of each solution and stirred (250 rev./min) for approximately 3 h. The quantity of absorbent was then reduced for the subsequent extraction procedures to identify the yield capacity of the absorbent. The solution was then filtered and the filtrates were collected.

A fixed-bed process was applied to mimic industrial applications: approximately 0.02 g of each silica sample was packed within a glass column (dimensions: 20 mm diameter and 25 cm length) through which 40 ml of each single metal ion in non-buffered water solution was passed. All filtered metal samples were then tested for the particular metal using atomic absorption spectroscopy (AAS). The remaining silica samples after extraction were analysed using nitrogen physisorption and scanning electron microscopy (SEM) to identify any changes in the surface area, pore size and morphology of the parent silica.

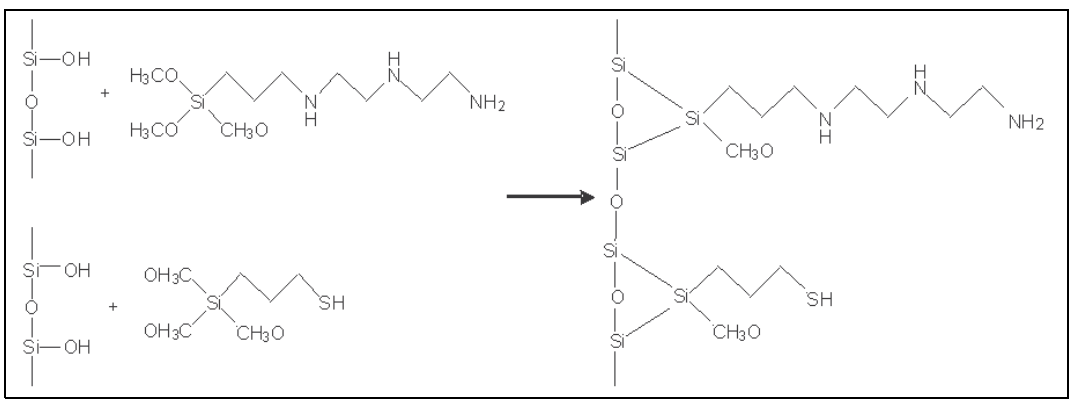

Figure 2.2. Schematic representation of the bi-functionalising procedure of mesoporous silica with aminopropyl and mercaptopropyl groups.

2.3.2 Extraction procedure for mixed metal ions

For application with environmental samples, mixed metal ion samples within a fixed-bed configuration process is more relevant. Inductively coupled plasma (ICP) standard mixed metal ion solutions were diluted to a 1 ppm solution using non-buffered water as a solvent. As reported previously, a glass column containing either the mono-functionalised or bi-functionalised mesoporous silica was used to filter approximately 10 ml of the 1 ppm mixed metal solution. The samples collected for each sample post-filtration were then examined on ICP to identify a reduction in the metal content. A comparable procedure was applied to an industrial sample supplied by the EPA.

2.3.3 Extraction procedure for gold nanoparticles

Gold nanoparticles were synthesised using 4 ml of 80 mmol tetraoctylammonium bromide ($C_{32}H_{68}NBr$) as a surfactant in toluene. The gold was sourced from a 30 mmol hydrochloric acid solution of gold ($HAuCl_4$). The mixture of the surfactant and the gold source was agitated within a separating funnel, and the resulting red layer containing the gold was collected. A 0.5 M sodium borohydride ($NaBH_4$) solution, a reducing agent, was then stirred with the gold source for 10 min. This mixture was then separated in a separating funnel and again the red layer containing the gold nanoparticles was collected and rinsed in a 0.1 M sulfuric acid solution (H_2SO_4). A 10 ml volume of a standard solution of known concentration of gold nanoparticles (calculated from sample mass) prepared in toluene was used for the extraction experiments. A 0.1 g quantity of blank silica, aminopropyl functionalised silica or mercaptopropyl functionalised silica was stirred (250 rev./min) in 10 ml of the solution containing gold nanoparticles for approximately 3 h. The mixtures were then filtered and the filtrates were collected. The absorbance of the filtered toluene solution was then measured using UV-Vis spectrometry (on a HP 8453 spectrometer). The remaining silica samples after extraction were analysed using nitrogen physisorption to identify any changes in the subsequent surface area and pore size post-extraction.

3 Results

3.1 Optimisation of the Pore Diameter in Mesoporous Silica Spheres

Many processes have been reported for increasing the pore diameter of mesoporous materials, including the addition of swelling agents, long-chain amines and the use of supercritical carbon dioxide (Blin *et al.*, 2000; Kruk *et al.*, 2000; Blin and Su, 2002). Blin *et al.* reported that the addition of swelling agents (decane and 1,3,5-trimethylbenzene) during the cetyltrimethylammonium bromide micellar preparation of mesoporous silica resulted in a pore diameter increase from 3.5 nm to 5.0 nm (Blin *et al.*, 2000; Blin and Su, 2002). Kruk *et al.* reported that the addition of large amounts of dimethyldecylamine restructures mesoporous silica (synthesised using cetyltrimethylammonium bromide) yielding an increase in pore size from 2.5 nm to 13.5 nm (Kruk *et al.*, 2000). Ammonia treatment also increases the pore size of mesoporous silicas synthesised with *n*-octyl-β-D-glucopyranoside, tetramethoxysilane and cetyltrimethylammonium bromide as studied by Xing and Rankin (2008). Use of these swelling agents has yielded, on average, a 30% pore size increase but also a loss in structure of the mesoporous phase (Park *et al.*, 2003). Supercritical carbon dioxide was applied by Hanrahan *et al.* for the controlled pore expansion within copolymer surfactant templated mesoporous silicas, resulting in pore diameters of up to 10 nm without a loss of ordering within the mesophase (Hanrahan *et al.*, 2004).

Pore expansion can also be achieved *via* manipulation of the chemicals used in the mesoporous silica synthesis procedure. Temperature increases during the synthesis procedure dictate an enlargement in the pore sizing of the material due to elevated hydrophobicity of the block copolymers in acidic solution (Copley, 2006). The confirmation of the oxyethylene group, within the PPO and PEO copolymer blocks, alters the hydrophobicity of the block copolymer. A gauche confirmation prevails at low temperatures but as the temperature increases the higher energy form is adopted which is the anti-confirmation giving rise to more hydrophobic synthesis. When using non-ionic block copolymer surfactants, an increase in the PPO block of the copolymer structure increases the pore diameter of the resultant mesoporous material (Flodstrom and Alfresson, 2003). This PPO block size increase is generally achieved through integration of two copolymers and also by increasing the overall surfactant content within the synthesis mix. Numerous studies have been conducted applying either one or both of these parameter changes to increase the pore size of mesoporous silica materials. Applying both of these methodologies gives a more facile method to generate larger pores within the mesoporous silica material, without introducing irrelevant chemicals to the basic synthesis procedure and, therefore, reducing the possibility of alteration to the silica phase or sphere morphology.

Yamada *et al.* (2002) employed temperature as the only variable throughout the synthesis procedure of mesoporous silicate powder to alter pore size. Two procedures were tested using either a P123 or an F127 copolymer with the temperature changes. Both hexagonal and cubic mesoporous silica spheres were synthesised with controllable porous phases. In this study, an increase in temperature resulted in an increase from 3.5 nm to 8.0 nm of the pore diameter.

Ryan *et al.* (2002) reported the synthesis of hexagonal mesoporous silica with tunable pore dimensions, achieved through mixing triblock copolymers while also increasing the overall copolymer content. Copolymers P123 and P85 were present within an acidic tetramethoxysilane (TMOS) mixture, at a 50 wt% surfactant concentration in comparison to the typical 1–10 wt% surfactant content. This method increased pore diameters in the range between 4.5 nm and 7.0 nm.

Ma *et al.* (2003) reported the synthesis of large-pore mesoporous silica spheres through the use of a triblock copolymer P123 in combination with a cosurfactant, cetyltrimethylammonium bromide

(CTAB), and a cosolvent, ethanol. The method of using a triblock copolymer and a cosurfactant for synthesising large-pore mesoporous silicas was also applied by Zhao *et al.* (1998). The addition of the cosolvent decreases the polarity of the solvent and thus decreases the rate of nucleation and growth of the mesostructured products because of the slower TEOS hydrolysis and mesostructure assembly, which could contribute to the formation of silica spheres with smooth surfaces. A two-step heating measure with varying ageing times was also used to control pore size within this synthesis (Zhao *et al.*, 1998).

The synthesis of cubic-phase mesoporous spheres is reported by Kim *et al.* (2004). Both triblock copolymers, P123 and F127, were used to attain certain molar compositions allowing for specific applications. The group reported that the mean pore diameter could be increased by increasing the content of the P123 copolymer in the polymer mixture. By varying the synthesis temperature, time and template composition, cubic mesoporous samples with essentially the same mesopore cage diameter and with largely different pore entrance sizes were synthesised.

In this study, mesoporous silica spheres were synthesised using non-ionic block copolymers. By increasing ageing temperature and the surfactant content within the synthesis, the successful synthesis of large-pore mesoporous silica spheres was achieved. Synthesising large-pore mesoporous silica particles with perfectly spherical morphology, monodispersivity and tailored pore size allows grafting of reagent chains into the pores which can then be applied as absorbents.

3.1.1 Results and discussion

Mesoporous silica sphere samples were synthesised through hydrolysing TEOS with hydrochloric acid using P123 and F127 as polymeric templates. Each sample synthesised was aged at two variable temperatures, 60°C and 110°C, and at varying times of between 1 and 7 days. The molar ratio of the synthesis was also altered by increasing the P123 polymeric template concentration from 3.68 to 5.35 g. The samples are denoted according to these variables, the prefix letter refers to molar composition for either 3.68 g P123 (A) or 5.35 g P123 (B), the temperature is then displayed followed by the length of ageing time in days, for example A60-1 refers to a sample containing 3.68 g of P123 aged at 60°C for 1 day. All samples were then filtered and calcined. The mesoporous silica spheres were characterised using XRD to identify the pore phase and d-spacing, SEM to identify the spherical morphology, and nitrogen physisorption to confirm the mesoporosity of each sample. The effects that the variations in synthesis have on the mesoporous spheres are identified using these characterisation procedures.

3.1.1.1 The effect of ageing temperature on pore size and morphology

The X-ray diffractograms of the calcined mesoporous silica sphere samples (aged at 60°C) are shown in Fig. 3.1. The XRD patterns correspond to a hexagonal mesophase structure with (100), (110) and (200) planes observed for the A60-4, A60-5 and A60-7 samples. The (100) plane is also evident for the A60-1, A60-2 and A60-6 samples but the (110) and (200) planes were not discernible. As the ageing time increases or decreases the (100) plane changes in intensity; sample A60-7 showed the strongest (100) reflection peak. The position of the (100) peak also varied between 0.89° 2θ for A60-1 and 0.90° 2θ for A60-7 samples.

The XRD patterns were also recorded for the calcined mesoporous silica sphere samples aged at 110°C,

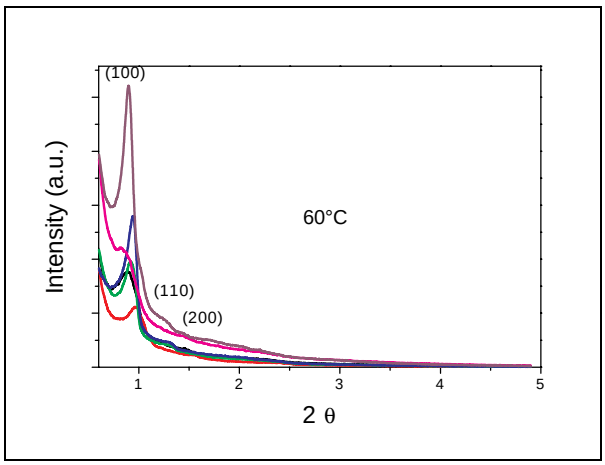

Figure 3.1. X-ray diffraction patterns for samples A60-1 (black), A60-2 (red), A60-4 (green), A60-5 (blue), A60-6 (pink), and A60-7 (purple).

shown in Fig. 3.2. The XRD patterns of the A110-2, A110-5 and A110-6 samples correspond to the hexagonal mesophase structure showing (100), (110) and (200) planes. The A110-1, A110-4 and A110-7 samples also display the (100) plane but the (110) and (200) planes have merged and are not resolvable. The (100) peak position alters for these samples between 0.88° 2θ and 0.81° 2θ for samples A110-1 and A110-7. The (100) reflection does not show the same pattern as seen in the sample aged at 60°C, and the A110-7 sample does not produce the most prominent (100) peak. It is the A110-5 sample that consistently showed the most prominent (100) peak. It can be concluded that the ordering of the pores for the 110°C samples was explicitly better than the pore ordering of the corresponding 60°C samples.

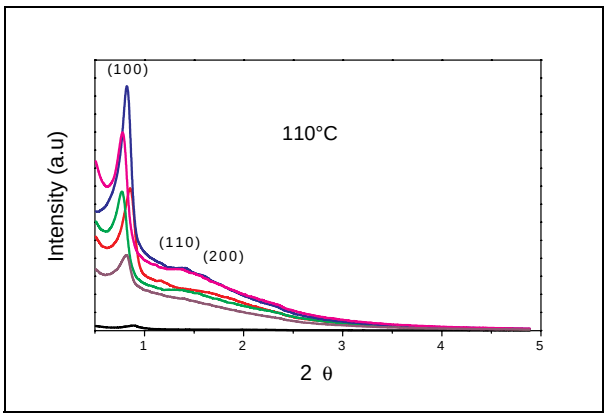

Figure 3.2. X-ray diffraction patterns for samples A110-1 (black), A110-2 (red), A110-4 (green), A110-5 (blue), A110-6 (pink), and A110-7 (purple).

The spherical morphology of the samples is witnessed by SEM analysis. Figure 3.3 shows the variation in the sphere morphology with increased ageing times for samples A60-1, A60-2, A60-4, A60-5, A60-6 and A60-7. A 2-day ageing step 60°C produces the best sphere profile.

Figure 3.4 shows SEM images of samples aged at 110°C. The temperature increase of the ageing step alters the sphere profile development and produces better sphere morphology. These SEM images show that sample A110-5 has superior sphere morphology when compared with all the other samples.

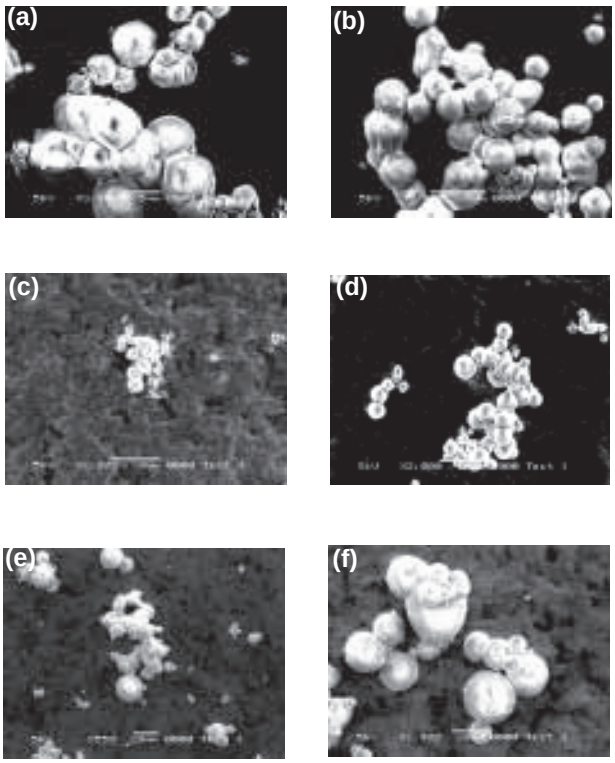

Figure 3.3. Scanning electron microscopy images of samples (aged at 60°C) (a) A60-1, (b) A60-2, (c) A60-4, (d) A60-5, (e) A60-6, and (f) A60-7 showing the spherical shape of each sample.

The porosity of the samples was investigated by nitrogen absorption. Most of the samples aged at temperatures of 60 and 110°C displayed distinctive Type IV isotherms characteristic of mesoporous material (Webb and Orr, 1997) as shown in Figs 3.5 and 3.6. Type IV isotherms can be further characterised into four types (Sing *et al.*, 1985), including the type H1 hysteresis loop, which displays parallel and nearly vertical isotherm branches typical for cubic mesoporous silica (Han *et al.*, 2004), and the type H2 hysteresis loop, displaying a triangular shape and a steep desorption branch typical of hexagonal mesoporous silica. The isotherms shown for samples aged at 110°C differ from those aged at 60°C. Samples A60-1, A60-5 and A60-7, shown in Fig. 3.5, have characteristics closer to the H2 hysteresis loop which is associated with uniform channel-like pores (Kruk *et al.*, 1997; Liu *et al.*, 1993). Sample A60-5 shows a step during desorption indicating disorder of the pore size. The A60-7 sample displays isotherm characteristics of

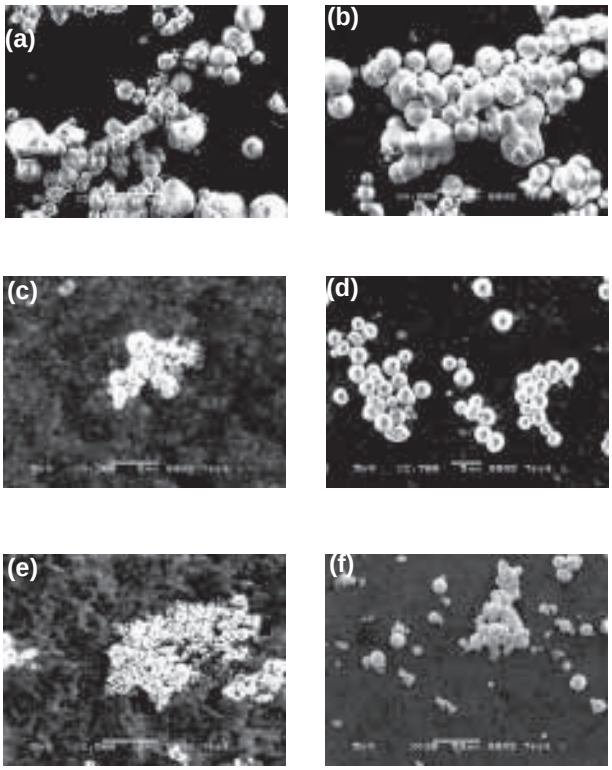

Figure 3.4. Scanning electron microscopy images of samples (aged at 110°C) (a) A110-1, (b) A110-2, (c) A110-4, (d) A110-5, (e) A110-6, and (f) A110-7 showing the sphere profile of each sample.

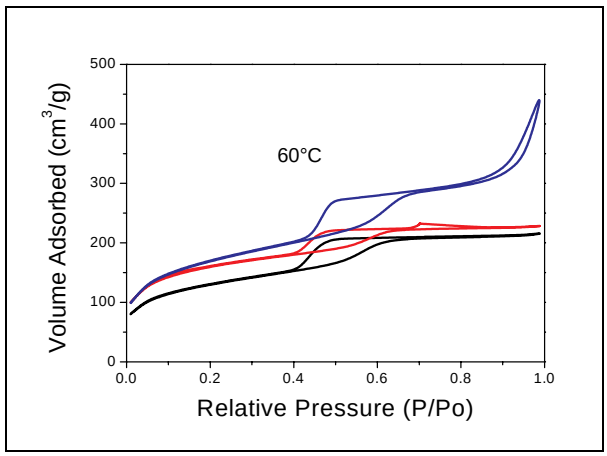

Figure 3.5. Nitrogen physisorption isotherms for samples A60-1 (black), A60-5 (red), and A60-7 (blue).

both mesoporous and macroporous phases. These factors highlight the inconsistency and unsuitability of these materials for chemical modification.

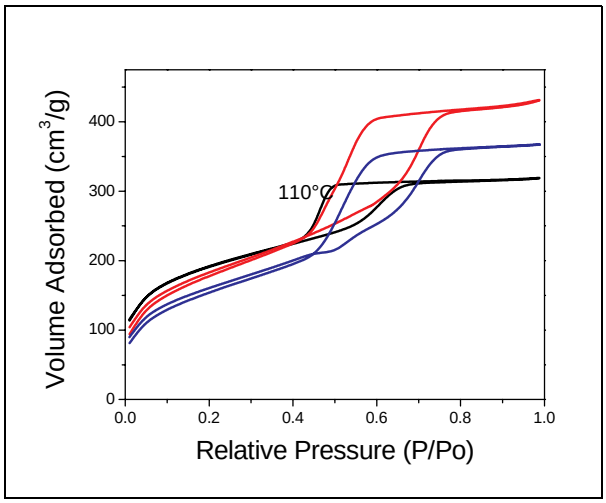

Figure 3.6. Nitrogen physisorption isotherm patterns for samples A110-1 (black), A110-5 (red), and A110-7 (blue).

Samples A110-1, A110-5 and A110-7 shown in Fig. 3.6 display characteristics of both the H1 and H2 hysteresis loops, depending on the ageing time. As the ageing time increases, from 1 to 5 days, the hysteresis loop displays branches more parallel and vertical, characteristic of H2 hysteresis, showing a possible change in pore phase with cylindrical pore geometry and a high degree of pore size uniformity (Huo *et al.* 1996; Kruk *et al.* 1997).

A pore size increase from 46 ± 6 Å to 55 ± 7 Å was observed for the 60°C aged samples as a function of an increase in ageing time (Fig. 3.7).

The pore distribution for samples A110-1, A110-5 and A110-7 are shown in Fig. 3.8. An increase in the mean pore diameter is evident in these samples with increasing ageing time, measuring at 51 ± 7 Å, 68 ± 10 Å and 66 ± 11 Å for samples A110-1, A110-5 and A110-7, respectively. The A110-7 sample also shows a second peak confirming the two pore sizes identified in the isotherm measurements.

The pore size of samples aged at both 60 and 110°C are shown in Fig. 3.9. Plotting the pore size of all 60°C-aged samples identifies an almost linear increase in pore size due to ageing time. The 110°C samples showed a distinct increase in pore size, levelling to approximately 67 Å for 4-, 5- and 7-day samples.

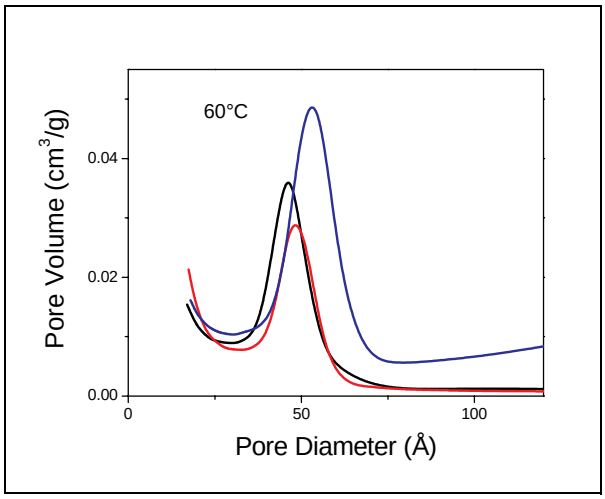

Figure 3.7. Nitrogen physisorption pore distributions for samples A60-1 (black), A60-5 (red), and A60-7 (blue).

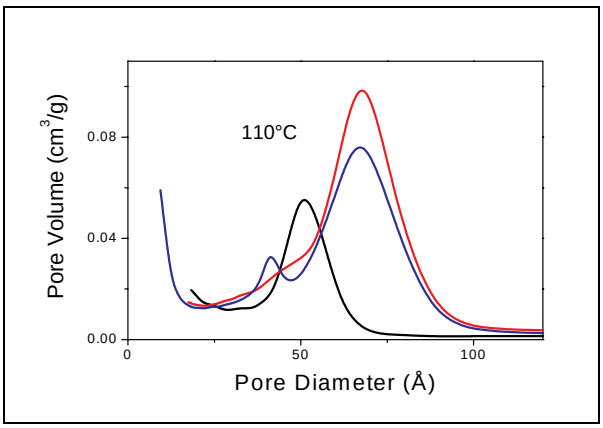

Figure 3.8. Nitrogen physisorption pore distributions for samples A110-1 (black), A110-5 (red), and A110-7 (blue).

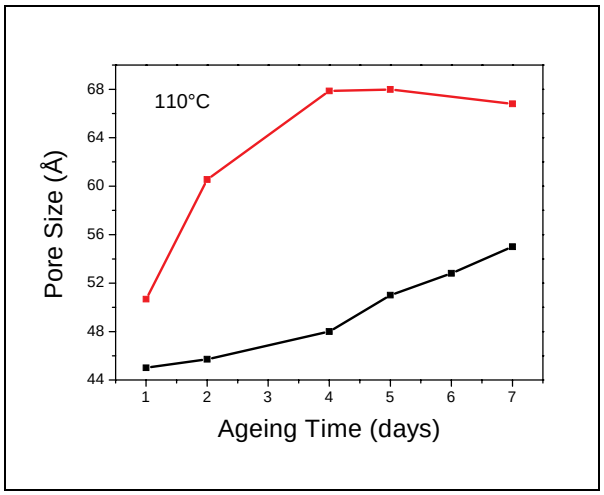

Figure 3.9. Pore size comparisons between A60 (black) and A110 (red) samples at each ageing time.

The increase in ageing temperature between the samples resulted in a pore diameter increase of 10 Å. These pore size increase results are comparable with those of previous reports as discussed in Section 3.2 (Kim *et al.*, 2004).

The physiochemical records for each sample synthesised are tabulated in Table 3.1, allowing a direct comparison of data in relation to ageing time and temperature.

A decrease in the (100) plane position measured by XRD is identified with both increasing ageing time and increasing ageing temperature. This decrease further corresponds to increasing d-spacing, matching the nitrogen physisorption results of larger pores. The

Table 3.1. Physiochemical data recorded for the mesoporous silica synthesised.

Ageing temp (°C)	Ageing time (days)	(100) (° 2θ)	d-spacing (Å)	Pore size (Å)	Surface area (m^2/g)	Pore volume (cm^3/g)
60	1	0.90	98	46	541	0.56
	5	0.94	94	48	444	0.65
	7	0.89	98	55	465	0.68
110	1	0.88	99	51	640	0.47
	5	0.82	107	68	642	0.67
	7	0.81	108	66	577	0.65

minimum pore size of 46 Å (A60-1 sample) is recorded at the lowest ageing time and temperature and a maximum pore size of 68 Å (A110-5 sample) is recorded at the highest ageing temperature. The surface area of the mesoporous spheres also increases with increasing pore diameter due to elevated ageing temperature. The pore volume decreases with temperature increase but increases with increasing ageing time. These results are evidence of the retention of the pore order and indicate that there is no pore collapse with variation of the synthesis process. Examining the SEM results highlights a significant improvement in the sphere profile with increasing temperature. At the elevated temperature, there is also a considerable improvement in the spherical morphology with ageing duration, the A110-5 sample producing the best sphere morphology. This may be attributed to the increased hydrophobicity of the surfactant at higher temperatures. These results allow us to conclude that the elevation of ageing/reaction temperature from 60°C to 110°C produces large-pore mesoporous silica spheres required for absorption.

3.1.1.2 The effect of P123 concentration on pore size and morphology

Increasing the ageing temperature and time during the synthesis of mesoporous silica spheres increases the mean mesopore diameter. Additionally, increasing the concentration of P123 copolymer in the reaction mixture is expected to enlarge the mean pore diameter due to the high ratio of the PPO block of this copolymer (Kim *et al.*, 2004). To investigate the effect of the P123 polymer content, the amount of P123 was increased from 3.68 to 5.35 g during synthesis and then aged at 110°C for between 1 and 7 days.

The diffraction patterns of both the 3.68 g and the 5.35 g P123 concentrated mesoporous silica samples, aged for 1 day at 110°C, are displayed in Fig. 3.10. Both samples exhibit narrow, uniform (100) reflections which is evidence of an ordered system.

The same comparison can be made between the 3.68 g and the 5.35 g P123 mesoporous silica samples aged for 5 days (Fig. 3.11). The hexagonal phase planes (100), (110) and (200) are notably better

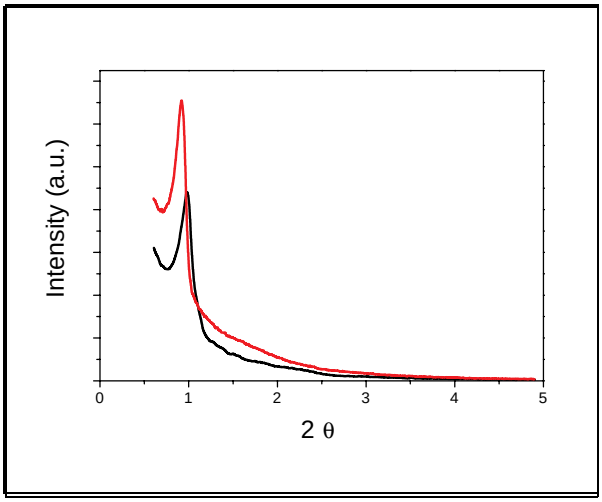

Figure 3.10. X-ray diffraction patterns (1-day ageing) for samples A110-1 (black) and B110-1 (red).

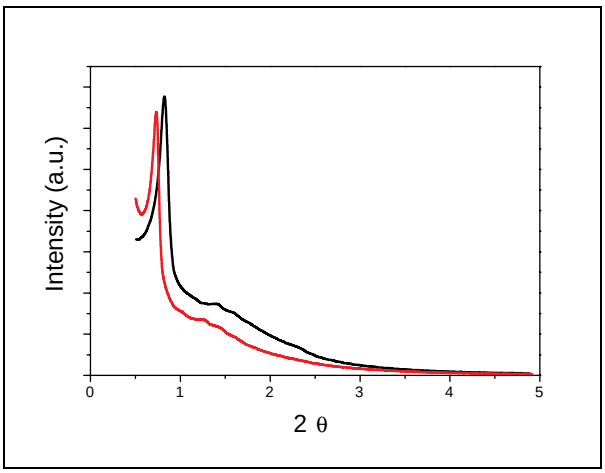

Figure 3.11. X-ray diffraction patterns (5-day ageing) for samples A110-5 (black) and B110-5 (red).

defined for these samples compared to the A110-1 and A110-5 samples shown in Fig. 3.10.

The (100) reflection plane for the samples aged for 7 days increases in intensity with increasing P123 content, as shown in Fig. 3.12. The (110) and (200) planes are also more evident for the B110-7 sample, indicating a possible increase in pore ordering with increased P123 content.

The sphere morphology of the samples does not significantly modify when the P123 content is

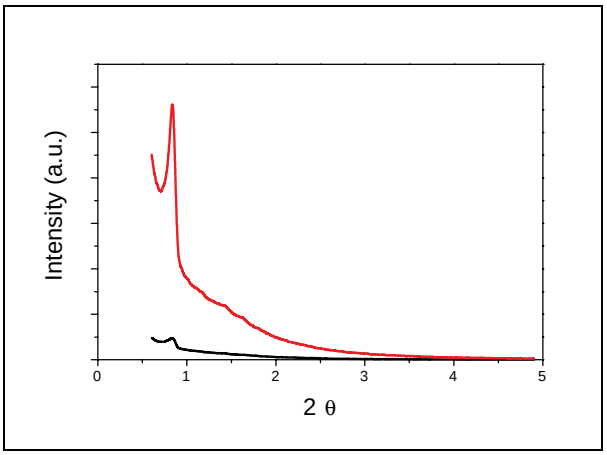

Figure 3.12. X-ray diffraction patterns (7-day ageing) for samples A110-7 (black) and B110-7 (red).

increased from 3.68 g to 5.35 g. The sphere profile is not evident for material aged for 1 day at 110°C, irrespective of surfactant concentration. The samples aged for 5 days show the best sphere profile with a sphere size increase with increased P123 content, as shown in Fig. 3.13 (c) and (d). The spheres aged for 7 days do not alter with P123 content but show increased agglomeration when compared to the samples aged for 5 days. These SEM images (Fig. 3.13) show that samples A110-5 and B110-5 have the best sphere morphology when compared to samples aged at different times.

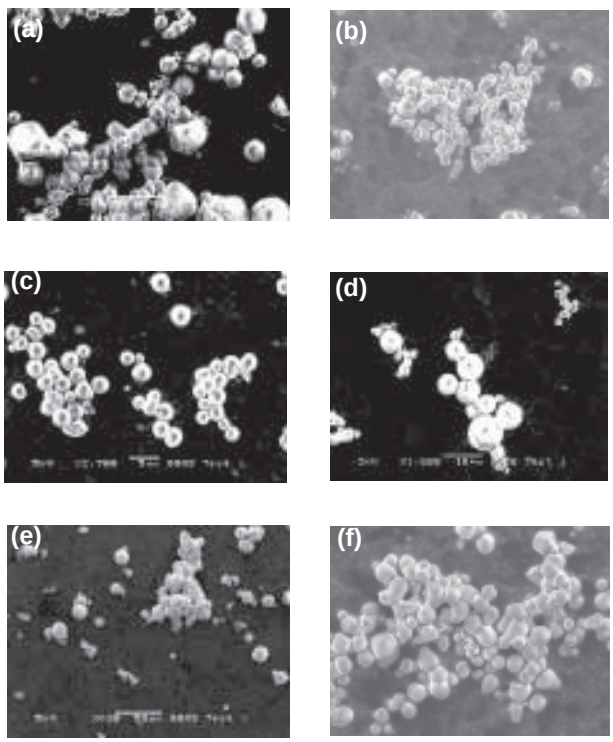

Figure 3.13. Scanning electron microscopy images of samples (a) A110-1, (b) B110-1, (c) A110-5, (d) B110-5, (e) A110-7, and (f) B110-7.

The nitrogen isotherm recorded for sample B110-1 shows a characteristic Type IV mesoporous isotherm (Fig. 3.14). On comparison of the A110-1 and B110-1 samples, it is evident that the mesoporous phase of the material is retained with only small alteration in the isotherms. There is evidence of a second step developing in the B110-1 sample, reflecting two pore sizes within the sample.

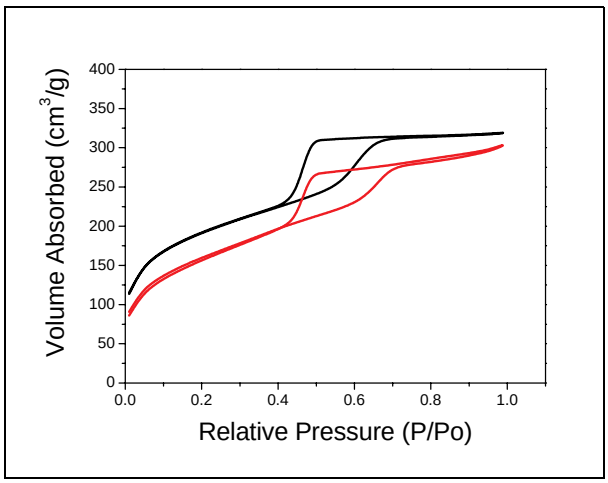

Figure 3.14. Nitrogen physisorption isotherm patterns (1-day ageing) for samples A110-1 (black) and B110-1 (red).

The pore diameter increase measured between the A110-1 and B110-1 samples, due to P123 surfactant increase, is shown in Fig. 3.15. Increasing the content of P123 from 3.68 to 5.35 g increases the mean pore diameter from 50 ± 7 Å to 60 ± 8 Å, confirming previous reports that the P123 content dictates the pore dimensions of mesoporous materials (Kim *et al.*, 2004).

Figure 3.16 illustrates typical nitrogen physisorption isotherms obtained from samples aged for 5 days with a P123 content of 3.68 and 5.35 g. Distinctive Type IV isotherms are observed in both cases. Further

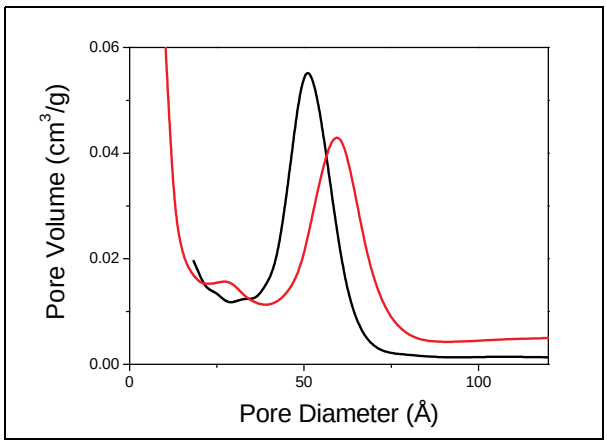

Figure 3.15. Nitrogen physisorption pore size distributions (1-day ageing) for samples A110-1 (black) and B110-1 (red).

physiochemical properties of these materials, including pore volume and surface area, are shown in Table 3.2.

Increasing the P123 content from 3.68 to 5.35 g shows a variation in the pore diameter of the A110-5 and B110-5 materials. Most markedly, the increase in copolymer content for samples A110-5 and B110-5 caused an increase in pore size from 68 ± 10 Å to 73 ± 11 Å, as shown in Fig. 3.17.

Figure 3.18 clearly shows that the samples aged for 7 days with differing P123 concentrations are all mesoporous as shown by the Type IV isotherm. Pore size distributions are shown in Fig. 3.19 and an increase in pore diameter from 66 ± 11 Å for sample A110-7 to 75 ± 11 Å for sample B110-7 was observed.

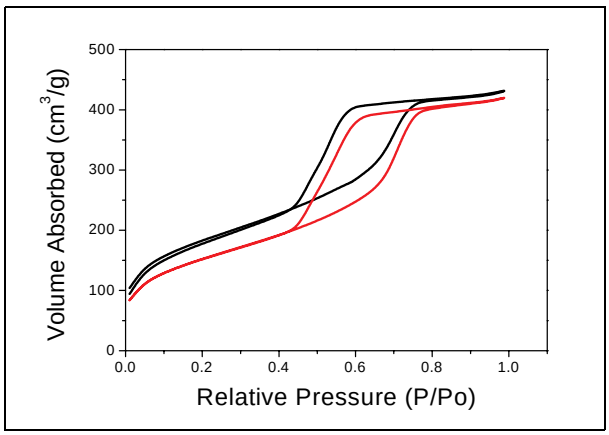

Figure 3.16. Nitrogen physisorption isotherm patterns (5-day ageing) for samples A110-5 (black) and B110-5 (red).

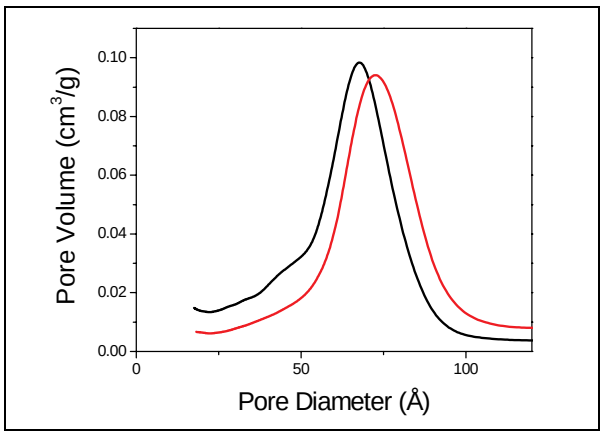

Figure 3.17. Nitrogen physisorption pore distribution curves (5-day ageing) for samples A110-5 (black) and B110-5 (red).

Table 3.2. Physiochemical data recorded for the mesoporous silica synthesised with increased P123 content.

P123 molar content (g)	Ageing time (days)	(110) (° 2θ)	d-spacing (Å)	Pore size (Å)	Surface area (m^2/g)	Pore volume (cm^3/g)
2.68	1	0.88	99	50	640	0.47
5.35	1	0.92	96	60	559	0.57
2.68	5	0.82	107	68	642	0.67
5.35	5	0.81	108	73	496	0.61
2.68	7	0.81	108	66	577	0.65
5.35	7	0.84	105	75	468	0.64

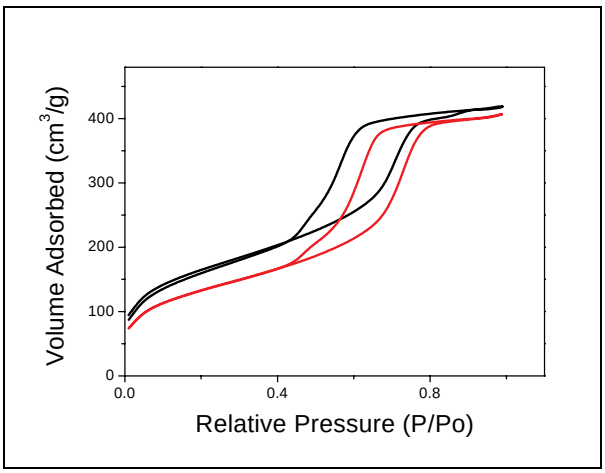

Figure 3.18. Nitrogen physisorption isotherm patterns (7-day ageing) for samples A110-7 (black) and B110-7 (red).

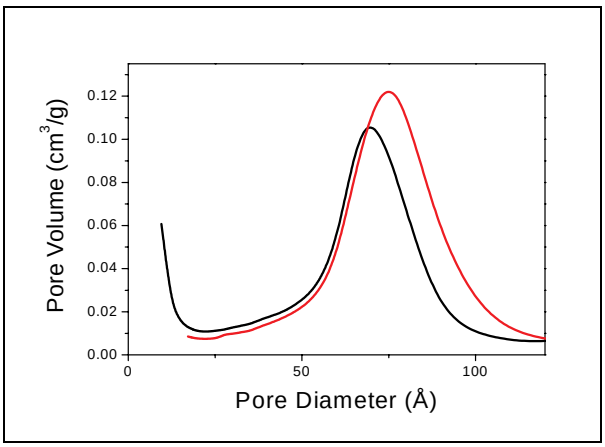

Figure 3.19. Nitrogen physisorption pore distribution curves (7-day ageing) for samples A110-7 (black) and B110-7 (red).

The physiochemical data recorded for each sample are illustrated in Table 3.2. The surface area decreases for the samples whilst the pore size increases. The pore size increase due to P123 content ranges between 6 Å and 10 Å.

3.2 Extraction of Metal Ions and Gold Nanoparticles from Solution Using Functionalised Mesoporous Silica Spheres

The conservation and protection of the environment are essential for the health of both humans and other organisms and, therefore, has increased the urgency for methods of removal of both metal ions and nanoparticles from the environment. Many methods for the removal of metal ions have been investigated, including precipitation, coagulation/flocculation, ion exchange, reverse osmosis (Bingau *et al.*, 1986) complexation/sequestration, and both electrochemical operation and biological treatment (Kiffs, 1987; Namasivayam and Ranganathan, 1995). However, limitations of many of these methods include high operating costs and large energy consumption. In the case of biological treatments, these systems are extremely sensitive to contamination and require constant monitoring. Use of absorptive compounds that can capture metal ions from solution, such as activated charcoal, zeolites and clays, has also been studied as waste-water treatment systems (Celik and Demirba, 2005). However, severe disadvantages are associated with the use of these materials as absorbents for metal ions, such as low loading capacities and relatively small metal ion binding constants. The erratic ion loading quantity from batch to batch of these materials causes unreliable results during applications.

Mesoporous materials are a relatively new material type that may have a wide application as absorbents owing to their large surface areas, large pore volumes and large pore diameters. The ability to control the morphology and pore diameter of mesoporous silica opens up possibilities for commercial application as metal ion absorbents. Facile functionalisation of mesoporous silica spheres, with different chelating agents or ligands, allows specific metal ion pollutants to be targeted and removed from aqueous or organic systems. From the Irving–Williams stability series, particular ligands form their most stable complexes with particular metal ions (Irving and Williams, 1953; Ahrland *et al.*, 1958). Further development of this work led to the development of Pearson's Hard–Soft Acid–Base (HSAB) Principle in which each metal and ligand are categorised so as to easily identify the most stable ligand–metal attractions. From Pearson's Principle, aminopropyl ligands (–NH) are identified as being effective ligands for binding to metal ions such as nickel, chromium, manganese and iron whilst mercaptopropyl ligands (–SH) readily bind to metal ions such as palladium and mercury (Pearson, 1963).

However, most environmental samples will contain a mixture of metal ions. Therefore, bi-functionalised mesoporous silica spheres with aminopropyl and mercaptopropyl ligand functionalities would allow removal of a diverse range of metal ions, i.e. both hard and soft metallic ions.

Many procedures for mono-functionalising mesoporous silica have been reported using a range of assorted ligands. For example, the functionalisation of mesoporous silica with a mercaptopropyl ligand, tris(methoxy)mercaptopropylsilane, for the extraction of mercury was reported by Fryxell *et al.* (1997). Mercier and Pinnavaia (1998) reported another approach for binding mercury metal ion by using 3-mercaptopropylsilyl-functionalised mesoporous silica. Northcott *et al.* (2006) have reported that silica functionalised with chloro ligands (*n*-octadecyltrichlorosilane) in toluene under reflux conditions can be used for the extraction of copper and zinc ions. Bois *et al.* (2002) reported that aminopropyl and mercaptopropyl functionalising mesoporous silica could be used to absorb copper, nickel and cadmium ions from pH 6 buffered solutions.

Procedures for bi-functionalising mesoporous silica using both aminopropyl and mercaptopropyl ligands have also been studied. For example, Mehdi *et al.* (2006) synthesised bi-functionalised silica through the co-condensation of dodecylamine-functionalised silica with aminopropyl or mercaptopropyl ligands. Zhang *et al.* (2004) reported a two-step bi-functionalising procedure where aminopropyl ligands were functionalised through co-condensation followed by a second functionalising step with phenyl ligands in supercritical carbon dioxide. These procedures used non-spherical mesoporous silicas. The synthesis of bi-functionalised mesoporous spheres has been reported by Zhu *et al.* (2005), using both co-condensation and post-synthesis refluxing procedures. In all of these reported studies, the functionalising procedure is extremely time consuming and laborious.

In this study, mesoporous silica spheres were functionalised following the experimental refluxing procedures. These functionalised spheres were subsequently used as absorbents for metal ions, both single metal and mixed metal solutions as well as metallic nanoparticles. Single metal ion extraction was carried out over the pH range between 4 and 10 to identify the optimum pH for removing each metal ion. Metal ion extractions were also carried out in non-buffered water to replicate the natural environmental conditions for these metal ions. The absorbents used for these extraction experiments consisted of mesoporous silicas functionalised with aminopropyl ligands (Si–NH), mesoporous silicas functionalised with a mercaptopropyl ligand (Si–SH) and mesoporous silicas functionalised with both aminopropyl and mercaptopropyl ligands (SH–Si–NH). Different metal ions form more stable complexes with either aminopropyl or mercaptopropyl ligands (Irving and Williams, 1953; Ahrland *et al.*, 1958). The hard aminopropyl ligand produces a stable ionic bond with hard metals such as chromium, nickel and iron, whereas the soft mercaptopropyl ligand results in a stable covalent bond with soft metals such as palladium and cadmium (Pearson, 1963). The use of the SH–Si–NH absorbent material allows a comparison of removal efficiency of single metal ions with either Si–NH or Si–SH. The absorbents were also used to remove mixed metal ion solutions in non-buffered water and in an environmental sample supplied by the EPA, to highlight the possibilities of using these materials for the clean-up of waste-water streams. Further to these experiments, both the parent silica samples and the functionalised silica samples were tested for their ability to remove gold nanoparticles from an organic solvent.

3.2.1 Chemical modification of the mesoporous silica surface

Scanning electron microscopy images of the blank mesoporous silica spheres (SiO_2), the aminopropyl (Si–NH) and mercaptopropyl (Si–SH)-functionalised spheres and the bi-functionalised (SH–Si–NH) samples are shown in Fig. 3.20. The spherical morphology is evident for both the blank and functionalised samples.

X-ray diffraction patterns of the calcined functionalised samples are shown in Fig. 3.21 and the data are summarised in Table 3.3. The hexagonal mesophase structure is preserved after functionalisation of the mesoporous spheres. The XRD patterns correspond to a hexagonal mesophase structure with (100), (110)

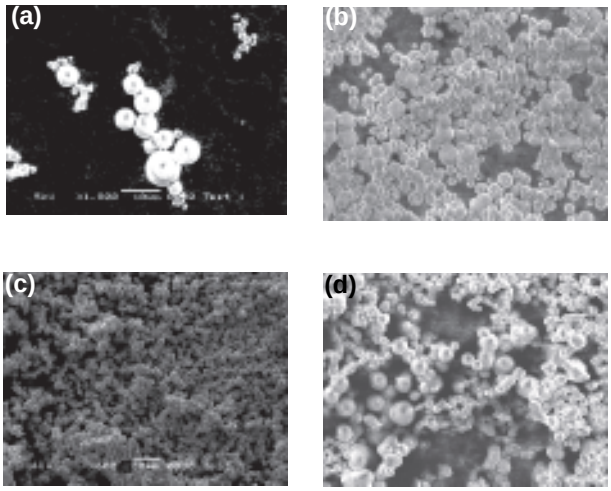

Figure 3.20. Scanning electron microscopy images of samples (a) SiO_2, (b) Si–NH, (c) Si–SH, and (d) SH–Si–NH showing the sphere morphology before and after functionalising.

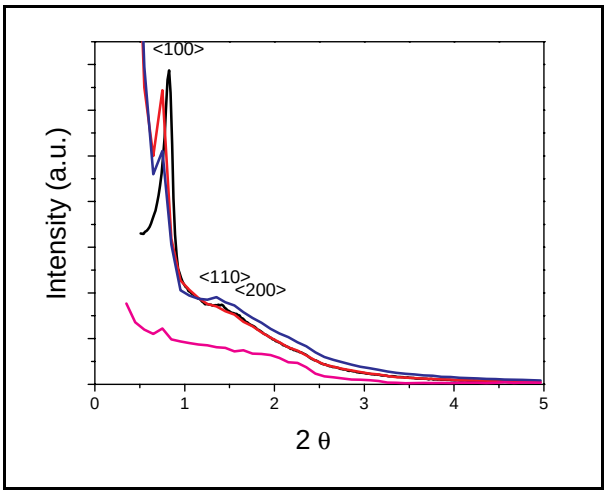

Figure 3.21. X-ray diffraction patterns of the SiO_2 (black), Si–NH (red), Si–SH (blue), and SH–Si–NH (pink).

Table 3.3. Physiochemical data recorded for the SiO_2, Si–NH, Si–SH and SH–Si–NH samples (values based on three batch products).

	Pore size (Å)	d spacing (Å)	Pore volume (cm^3/g)	Surface area (m^2/g)	P/Po
SiO_2	76	168	0.629	706	0.451
Si–NH	53	55	0.313	119	0.411
Si–SH	67	58	0.586	703	0.414
SH–Si–NH	50	48	0.085	85	0.405

and (200) reflections. The (100) peak occurs at 0.83° 2θ, 0.75° 2θ, 0.77° 2θ and 0.74° 2θ for the SiO_2, Si–NH, Si–SH and SH–Si–NH, respectively. After functionalisation, the intensity of the (100) reflection decreases dramatically for all the samples due to either a loss of order or a loss in contrast due to the functional groups.

Figure 3.22 illustrates typical Type IV nitrogen-absorption isotherms obtained from the blank and functionalised mesoporous spheres. All of the samples have distinct hysteresis loops and steep absorption/desorption steps, indicating an ordered array of mesopores consistent with the XRD profiles. All samples displayed parallel and nearly vertical isotherm branches typical of hexagonal mesoporous silica. The Type IV isotherm shape is preserved for all

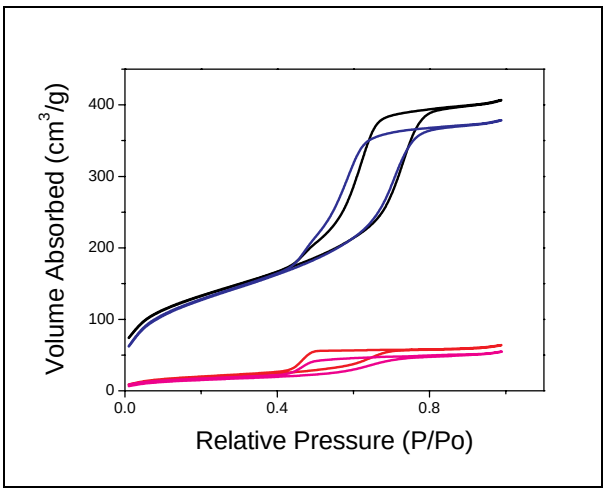

Figure 3.22. Nitrogen physisorption isotherm patterns of the SiO_2 (black), Si–NH (red), Si–SH (blue), and SH–Si–NH (pink).

samples suggesting that the mesoporous structure has been maintained post-functionalisation. Previous studies report reduced distinction of the absorption step suggesting some loss of structure regularity (Zhu *et al.*, 2005). All functionalised samples showed a reduction in the effective pore diameter, indicating a coating of the pore wall.

The mean pore diameter, pore volume and surface area calculated from the Barrett–Joyner–Halenda (BJH) model are described in Table 3.3 and the data are plotted in Fig. 3.23. Functionalisation has a dramatic effect on the pore diameter and volume. In the case of the aminopropyl-treated silica, the pore diameter shifts from 76 Å to 53 Å and the pore volume changes from 0.629 to 0.313 cm^3/g. Aminopropyl functionalisation reduces the pore diameter (from 76 Å to 53 Å) and pore volume (from 0.629 cm^3/g to 0.313 cm^3/g) by significantly more than the mercaptopropyl treatment (from 76 Å to 67 Å and from 0.629 cm^3/g to 0.586 cm^3/g). These value reductions are due to the significantly greater length of the hydrocarbon chain and the increased loading of the aminopropyl species. The bi-functionalised system has the lowest effective pore diameter (50 Å), pore volume (0.085 cm^3/g) and surface area (85 m^2/g).

Elemental analyses of the silica samples after functionalising were used to further quantify the bonding and uptake of aminopropyl (–NH) and mercaptopropyl (–SH) moieties grafted to the silica following functionalisation. Table 3.4 compares the percentage carbon, hydrogen, nitrogen and sulfur (by weight) measured for the original blank mesoporous sample against the aminopropyl and mercaptopropyl-functionalised samples. The C/H/N ratio determined for the aminopropyl-functionalised material was 10.3:23.5:3 consistent with bonding to the surface

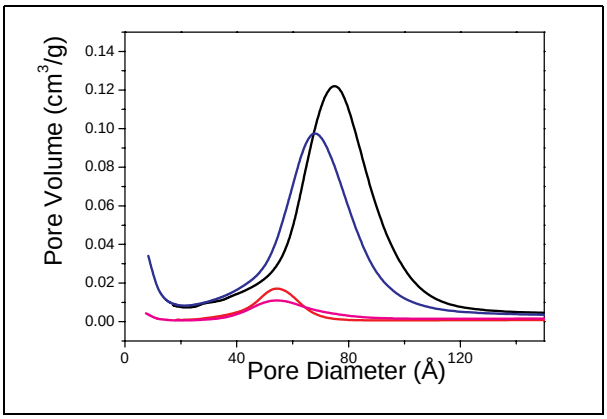

Figure 3.23. Nitrogen physisorption pore size distribution patterns of the SiO_2 (black), Si–NH (red), Si–SH (blue), and SH–Si–NH (pink).

through the methoxy group and the release of methanol during functionalising. For the mercaptopropyl-functionalised samples, the C/H/S ratio was determined as 3:7.8:0.98, close to that expected by the loss of the three terminal methoxy groups and bonding to the surface. The attachment of the ligand at the methoxy is reported as the most common attachment technique. Importantly, the co-functionalisation does not alter the elemental compositions (within experimental error), suggesting that the additions are purely additive.

The bonding of the functional groups to the surface of the pore walls is through reaction with surface silanol (Si–OH) groups. Figure 3.24 shows the infrared spectra measured for each of the samples between 4,000 and 1,300 waves/cm. For the silica sample, a sharp absorption band is identified at 3,745 waves/cm due to free Si–OH groups while the broad absorption band at 3,410 waves/cm is assigned to hydrogen-bonded Si–OH groups (Bois *et al.*, 2002). Both these

Table 3.4. Elemental analysis data recorded for the SiO_2, Si–NH, Si–SH and SH–Si–NH (values based on three batch products).

	Carbon %	Hydrogen %	Nitrogen %	Sulfur %
SiO_2	0.35	0.11	0	0
Si–NH	11.31	1.98	3.7	0
Si–SH	3.44	0.67	0	2.71
SH–Si–NH	14.38	2.55	3.86	2.74

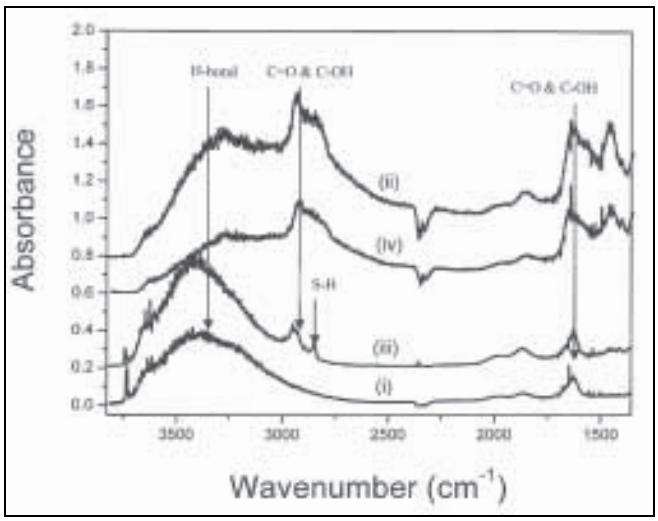

Figure 3.24. Fourier-transform infrared spectra of (i) SiO_2, (ii) Si–NH, (iii) Si–SH, and (iv) SH–Si–NH samples.

bands are strongly attenuated by functionalisation. For the aminopropyl-functionalised materials, isolated silanol groups were not observed but a broad band was distinguished at 3,250 waves/cm which can be assigned to hydrogen-bonded species associated with the remaining methoxy groups. New features can also be seen at 2,700–2,900, 1,625 and 1,460 waves/cm which can be assigned to C=O and C–OH stretches of the methoxy groups (Bois *et al.*, 2002). There is another, just, resolvable feature around 1,300 waves/cm which can be assigned to C–H bending of the methoxy groups. The mercaptopropyl-functionalised materials show almost complete loss of the silica silanol groups at 3,740 waves/cm and attenuation of the hydrogen-bonded Si–OH groups (3,440 waves/cm). The feature observed at 3,627 waves/cm can be attributed to a weak v (S–H) vibration (Socrates, 1994).

3.2.2 Absorption of individual metal ions

Each absorbent (Si–NH, Si–SH and SH–Si–NH) was tested for its ability to absorb Cr^{6+}, Ni^{2+}, Pd^{2+}, Fe^{2+} and Mn^{2+} ions at pH values of 4, 7 and 10. Metal ion species can be highly dynamic and their oxidation state may change with respect to different surrounding parameters, including pH. This separation of oxidation states is referred to as metal ion speciation. To counteract the effect of possible metal ion speciation within the different experimental solutions, calibration curves were measured for each metal ion at each pH. These calibration curves are not reported at this point but each one measured R^2 values of between 0.998 and 0.999. This means that all results reported here are true values irrespective of ion speciation. Absorption tests were also carried out in non-buffered aqueous solution in an attempt to model the extraction profile of the absorbent working under natural conditions. The pH value of the metal ions in the non-buffered aqueous solution is measured at approximately pH 3. A control experiment using the unfunctionalised parent SiO_2 as an extraction material yielded negligible results, removing less than 1 ppm for all metals. The initial concentration of all metals was standardised at 10 ppm due to atomic absorption spectroscopy constraints.

A direct comparison between the remaining single metal ions after extraction using Si–NH as the absorbent is shown in Table 3.5. As expected the Si–NH materials show a large capacity for iron, manganese, nickel and chromium, with increasing metal loading noticeable at the more basic side of the pH scale. Metal ion loadings shown compare very well to industrial absorbents. Indeed literature values for nickel show loading capacities of only 150 µmol/g (Bois *et al.*, 2002), in which functionalised silicas with a smaller pore size were also used as absorbents. Si–NH showed negligible affinity for palladium as expected due to the soft nature of the palladium ion.

Table 3.5. Absorption capacity (µmol/g) of metal ions at varying pH values and aqueous solutions using Si–NH as the absorbent. Values are based on an average of three extraction results.

Metal	pH 4	pH 7	pH 10	Water
Nickel	76	340	340	340
Chromium	354	322	384	360
Iron	0	358	358	358
Manganese	0	364	364	364

As expected no uptake is observed for iron, chromium, nickel or manganese when Si–SH is used as the absorbent; however, significant quantities of palladium are extracted. Table 3.6 depicts the absorption capacity of Si–SH for palladium as a function of pH. More neutral solutions of pH 7 and non-buffered aqueous solutions favour the extraction of palladium. The results recorded for palladium removal compare well with previously reported data; Kang *et al.* (2004) reported maximum removal of palladium using mercaptopropyl (3-mercaptopropyltrimethoxysilane)-functionalised mesoporous silica to be 92 µmol/g.

Table 3.6. Absorption capacity (µmol/g) of Si–SH for palladium at varying pH values and as prepared (i.e. no buffer) solutions. Values are based on an average of three extraction results.

Metal	pH 4	pH 7	pH 10	Water
Palladium	186	187	114	187

The measured higher attachment of the nickel, chromium, manganese and iron metal ions to the Si–NH absorbent and the palladium metal ion to the Si–SH absorbent can be explained by the co-ordination of each metal ion.

The maximum co-ordination of Ni^{2+} ions is 6, therefore falling within the octahedral structure set. In this form, aminopropyl ligands displace some or all of the water molecules within the octahedral ion $(Ni(H_2O)_6)^{2+}$ and forms a complex such as *trans*-$(Ni(H_2O)_2(NH_3)_4)(Ni_3)_2$ (Cotton and Wilkinson, 1966). This complex will form between the aminopropyl-functionalised silica and the nickel ions during the extraction process.

The aqueous chemistry of hexavalent chromium is very important; in acidic solutions a dichromate ion structure is formed, $(Cr_2O_7^{2-})$, whereas within a more basic solution it forms a tetrahedral chromate ion, (CrO_4^{2-}). The dichromate ion complex bonds with aminopropyl ligands and forms the structure $(NH_4)_2Cr_2O_7$.

Iron ions form a number of complexes, the majority of which can be classified as octahedral structures, and are unstable within aqueous solutions except when chelating with aminopropyl ligands, forming stable complexes (Cotton and Wilkinson, 1966). This stable complex explains the removal of the iron ions as the iron ions bond with the aminopropyl ligands attached to the silica surface.

The manganese ion is larger than the previously discussed ions and is not effectively stabilised with ligands. When manganese ions are in aqueous solution they are hydrated and contain $(Mn(H_2O)_6)^{2+}$. The aqueous ions can react with chelating ligands, resulting in structures such as $(Mn(NH_3)_6)^{2+}$.

Palladium ions are the only metallic ions in this research that form a stable bond with the single mercaptopropyl-functionalised mesoporous silica. Within the standard solutions the palladium ions are dissolved in an aqueous HCl solution, yielding $(PdCl_4)^{2-}$ ions. This attached chloride also reacts with the mercaptopropyl ligand.

Table 3.7 shows the absorption capacities for the bi-functionalised sample SH–Si–NH. Significant loading of both hard and soft metallic ions is noticeable. Similar

Table 3.7. Absorption capacity (µmol/g) of SH–Si–NH for metal ions at varying pH values and extraction results under neutral (water) conditions (values based on three extraction results).

Metal	pH 4	pH 7	pH 10	Water
Nickel	114	340	340	340
Chromium	258	258	278	362
Iron	117	358	358	358
Manganese	0	364	364	152
Palladium	188	188	188	188

metal ion loadings to singly functionalised samples are noticeable, as expected from elemental analysis shown in Table 3.4. The increased loadings identified in comparison to previously reported materials are due to the larger pore size available within the functionalised mesoporous silica sphere used in this study.

Table 3.8 illustrates the physiochemical properties of the absorbents after the extraction procedure. This yields further evidence of the metal ion attached within the pore of the chosen functionalised silica and is shown with the changing properties of the original functionalised silica samples post-filtration. Significant decreases in surface area are noticeable after the extraction; in the case of palladium extraction using Si–SH, a minuscule surface area remains after extraction.

Table 3.8. Physiochemical data recorded for the metal–silica composites post-extraction.

	Pore size (Å)	Pore volume (cm^3/g)	Surface area (m^2/g)	P/Po
Si–NH	52.5	0.313	119	0.41
Si–SH	67	0.586	703	0.41
Si–NH–Ni	50.5	0.102	61.3	0.41
Si–NH–Cr	48.1	0.276	105.3	0.41
Si–NH–Fe	51.7	0.012	12.7	0.11
Si–NH–Mn	50.1	0.087	56.4	0.36
Si–SH–Pd	44.6	0.018	3.2	0.31

3.2.2.1 Fixed-bed process extraction results

For a more industrial application, each absorbent was tested using a fixed-bed process and each metal ion solution was filtered through a packed column under gravitational pressure. Each absorbent used previously in the stirring experiments was packed within the column (allowing a comparison between the efficiency of the experimental procedures), while a standard quantity of 10 ppm was prepared of each metal in non-buffered water.

Table 3.9 shows the quantity of each single metal absorbed using Si–NH for nickel, chromium, iron and manganese, Si–SH for palladium, and SH–Si–NH for all five metal ions using the column filtration procedure.

Table 3.9. Absorption capacity (µmol/g) of SH–Si–NH for metal ions in water.

	Si–NH or Si–SH	SH–Si–NH
Nickel	340	201
Chromium	384	384
Iron	358	159
Manganese	365	84
Palladium	188	188

There is an evident reduction in sorptive capacity between the mono-functionalised and the bi-functionalised silica. As the bi-functionalised silica has a smaller effective pore size the metal ion solution may necessitate a longer interaction time with the material than is given during this experimental procedure. These results are significantly superior to previously reported extraction results (Bois *et al.*, 2002; Kang *et al.*, 2004; Unob *et al.*, 2007; Uysal and Ar, 2007).

Figure 3.25 compares the two extraction procedures reported in the experimental section. Both experimental procedures (stirring and column) evaluated here use the Si–NH or Si–SH absorbent material. When examining the column filtration extraction results it is evident that there is no loss in extraction efficiency, each metal is removed as efficiently or more efficiently in association with the stirring filtration extraction results. This emphasises the appropriateness of both this material and the extraction procedure for industrial applications.

The extraction results recorded when using SH–Si–NH for both the stirring and column filtration experimental procedures are shown in Fig. 3.26. With the SH–Si–NH absorbent there is an obvious reduction in extracting nickel and iron ions yet identical or increased extraction for chromium, manganese and palladium ions when applying the column filtration system as opposed to the stirring procedure. This corroborates what was seen previously, i.e. with the smaller effective pore size available within the SH–Si–NH absorbent, increased interaction time between the nickel and iron ion solution and the absorbent is required.

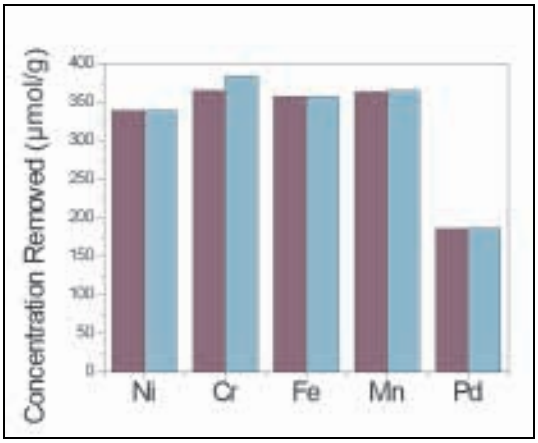

Figure 3.25. Metal ion extraction results (µmol/g) for Si–NH or Si–SH using the stirring (purple) and fixed-bed filtration (cyan) procedures.

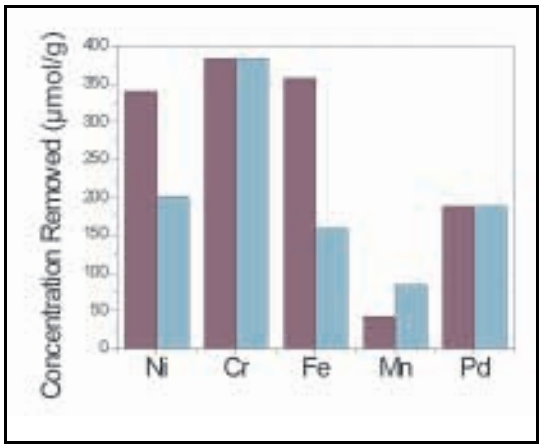

Figure 3.26. Metal ion extraction results (µmol/g) for SH–Si–NH using the stirring (purple) and fixed-bed filtration (cyan) procedures.

3.2.3 Absorption of mixed metal ions

Following the removal of individual metal ions from solution, extraction studies were undertaken on solutions containing more than one metal ion. In these studies, a facile fixed-bed filtration system was also used. Table 3.10 shows the absorption capacities of the mono-functionalised and bi-functionalised materials used for 1 ppm standard mixed metal solutions.

The mixed metal ion sample was dissolved in a non-buffered aqueous solution for two reasons:

1. The single metal ion removal experiments showed that the extraction efficiency was maximum when using a non-buffered aqueous solution as a solvent, and

Table 3.10. Inductively coupled plasma data recorded pre- and post-extraction of mixed metal ions (µmol/g) using Si–NH, Si–SH and SH–Si–NH. Extractions were carried out in non-buffered aqueous solutions (values based on the mean of three extraction results).

	Initial concentration (µmol/g)	Si–NH	Si–SH	SH–Si–NH
Zinc	153.9	0.6	30.8	1.3
Lead	48.3	0	7.7	1.3
Cadmium	88.9	0.8	13.1	0.1
Nickel	170.4	16.0	30.1	3.4
Iron	179.1	1.6	17.3	0.2
Chromium	193.3	18.9	26.5	3.2
Magnesium	411.4	338.1	75.2	0
Vanadium	196.3	7.0	6.7	0
Manganese	183.0	3.5	27.6	0
Calcium	249.5	93	25	3.8
Copper	157.4	0	0	0

2. An aqueous solution gives a similar solution to environmental samples. The pH of a mixed metal ion sample within an aqueous solution was measured at a value of 3.3.

As each single metal ion is attracted to different mono-functionalised mesoporous silica, using bi-functionalised mesoporous silica will allow a mix of metal ions to be removed from one solution. The Si–NH material showed large extraction capacities for zinc, lead, cadmium, nickel, iron, chromium, manganese and copper ions whereas the Si–SH material shows a preferential extraction of magnesium, vanadium and calcium ions. The SH–Si–NH material showed an extraction ability for each metal within the solution, emphasising its suitability for extracting metal ion pollutants from industrial samples. When using the ICP analysis equipment, the largest quantity measurable is a 1 ppm mixed metal solution, but these recorded data can be applied for increased quantities.

3.2.4 Extraction of metal ions from an industrial sample

Since the efficiency and suitability of each functionalised mesoporous silica absorbent has been examined and substantiated, the next step was to use *in vitro* metal ion samples. These experiments showed how effective the absorbents were at extracting metal ions from an industrial water sample, sourced from landfill leachate, supplied by the EPA. The sample was filtered through each absorbent packed within the glass column as reported previously. Table 3.11 shows the metal ion quantities measured within the environmental sample pre- and post-filtration through each absorbent as measured using ICP.

Seven metal ions were identified within the original environmental sample, varying greatly in concentration. Each metal was then bonded to a particular absorbent although some attractions oppose what was identified using the *in vitro* prepared mixed metal ion sample. The Si–NH absorbent formed stronger bonds with nickel, iron, chromium and manganese ions whereas the Si–SH absorbent bonded with zinc and vanadium ions. The SH–Si–NH absorbent does not yield the most efficient results when applying the environmental sample. This extraction reduction is possibly due to the smaller pore sizing accessible to the sample, the unpredictable nature of the metal ion interactions within the *in vivo* sample used or the reduced contact time with the sample within the column system. Figure 3.27 shows visual removal of pollutants from the initial environmental sample for each absorbent material used. From this visual inspection, the Si–NH material is highlighted as removing many other visual pollutants (not associated with metal ions) from the solution, resulting in an unsoiled sample when compared with the other materials.

Table 3.11. Inductively coupled plasma data recorded pre- and post-extraction of environmental sample (µmol/g) using Si–NH, Si–SH and SH–Si–NH extraction carried out in a non-buffered aqueous solution (values based on an average of three extraction results).

	Environmental sample (µmol/g)	Si–NH	Si–SH	SH–Si–NH
Zinc	7.76	3.43	1.09	7.36
Nickel	13.03	7.47	8.69	10.08
Iron	521.20	8.17	36.56	92.37
Chromium	37.65	15.32	16.14	16.48
Vanadium	13.26	5.8	3.43	4.56
Manganese	219.72	12.59	53.48	59.94
Calcium	1,323.38	190.55	190.55	190.55

Figure 3.27. Visual of extraction of pollutants within the industrial sample. (i) Original industrial sample, (ii) filtered through Si–NH, (iii) filtered through Si–SH, and (iv) filtered through SH–Si–NH.

3.2.5 Extraction of gold nanoparticles

Three materials synthesised (Si, Si–NH and Si–SH) were used as an absorbent for the gold nanoparticles in toluene solutions. The extraction results are shown in Fig. 3.28, in comparison with the standard original solution used prior to the filtration experiment. To ensure that the reduction is not due to nanoparticle agglomeration, the original nanoparticle standard was re-tested and showed no peak reduction from the initial UV-Vis result.

The extraction of the gold nanoparticles is maximum when using blank silica when compared with both other absorbents applied. This is possibly due to the larger pore sizing available to the gold nanoparticles allowing a higher quantity of gold to penetrate into the pores of the silica spheres. The Si–SH absorbent shows high affinity to the gold nanoparticles as opposed to the Si–NH absorbent. Figure 3.29 shows the visual effect of filtration. It is extremely challenging to disperse nanoparticles evenly within a solvent and therefore quantification of the nanoparticles extracted is undependable. However, from the UV-Vis results, the extraction quantities can be approximated at

Figure 3.29. Visual absorbance of (1) standard gold nanoparticles, (2) post-Si–NH extraction, (3) post-Si–SH extraction, and (4) post-Si extraction.

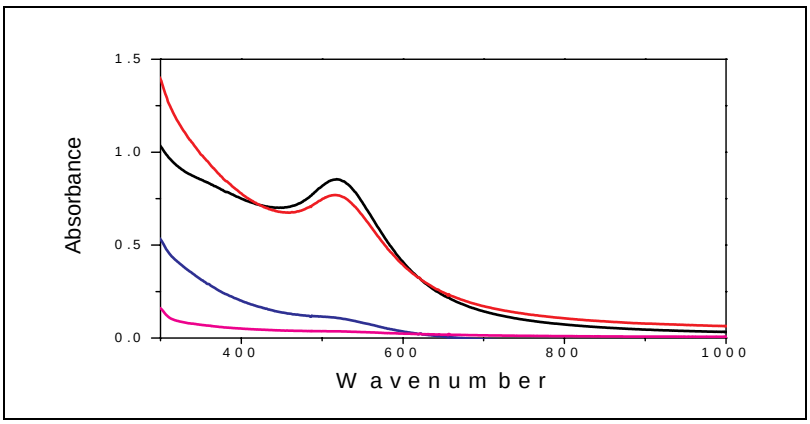

Figure 3.28. UV-Vis absorbance measurements of standard gold nanoparticles (black), post-Si–NH extraction (red), post-Si–SH extraction (blue), and post-Si extraction (pink).

0.1203 M of gold nanoparticles per gram with Si, 0.0112 M/g with Si–NH, and 0.1091 M/g with Si–SH.

To further confirm the addition of the gold nanoparticles within the pore of the mesoporous silica spheres, nitrogen physisorption analysis was used to identify any material alterations. Figure 3.30 depicts the Type IV isotherms obtained from the samples used for gold nanoparticle extraction. The distinct hysteresis loops and absorption/desorption steps are attained post-extraction, highlighting the lack of pore blockage and retention of the well-ordered pore structure in materials containing gold nanoparticles.

A minimal reduction in pore size is also recorded using nitrogen physisorption, shown in the pore distribution curves (Fig. 3.31). The largest decrease in pore size and pore volume is recorded for the non-functionalised silica material (Si–Au) containing gold nanoparticles, a reduction from 72 Å to 65 Å in pore size and from 0.095 to 0.052 cm^3/g for pore volume, reflecting the extraction results recorded using UV-Vis. As previously recognised, the Si–SH material removes more of the gold nanoparticles than the Si–NH material, due to the soft nature of gold, and this is again identified in the nitrogen physisorption results, with pore size and pore volume of the Si–SH material reducing further than the Si–NH material.

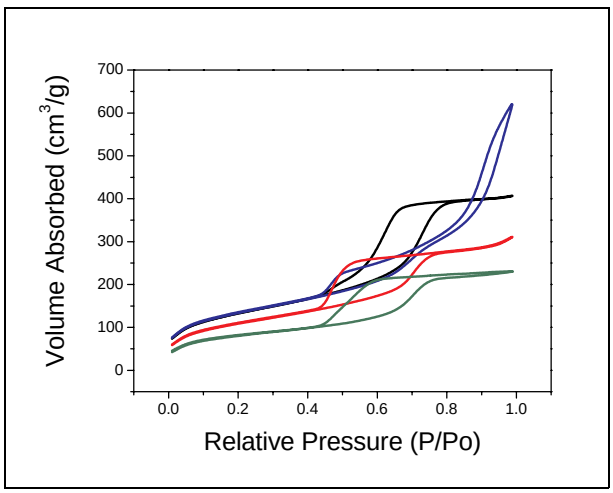

Figure 3.30. Nitrogen physisorption isotherms of SiO_2 (black), Si–Au (blue), Si–NH–Au (red), and Si–SH–Au (green).

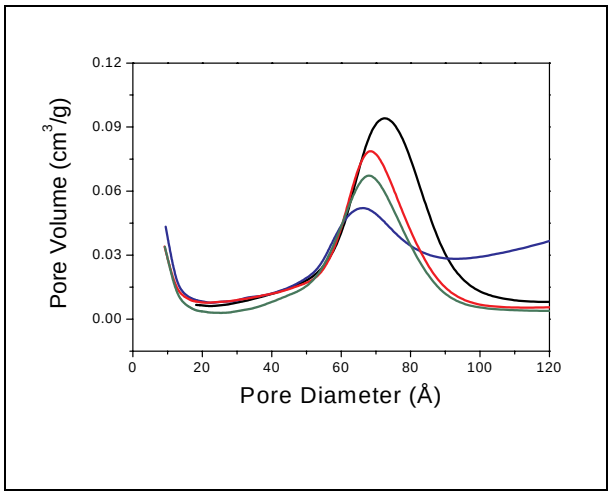

Figure 3.31. Nitrogen physisorption pore size distributions of SiO_2 (black), Si–Au (blue), Si–NH–Au (red), and Si–SH–Au (green).

4 Conclusion

There has been a lot of interest in mesoporous silica material since its synthesis procedure was developed and reported by Beck *et al.* in 1992. Since this mesoporous material discovery there have been extraordinary advances in synthesis procedures, leading to the finding of different material forms, including mesoporous silica bulk powders, thin films and spheres. The interest shown in mesoporous silica material is also due to its adaptability for different applications, including catalysis, sensing, molecular sieving, templating of nanostructures and in separation and absorption processes. Research at UCC has been significantly involved in furthering the knowledge of each of the mesoporous silica material forms while also exploring many different applications of the material. The work included in this study is focused on the production of mesoporous silica spheres and highlights how synthesis parameters and process conditions can significantly alter the material's final structure. It additionally reports on three different applications of the resultant material in both the environmental and analytical chemistry areas.

The synthesis process for mesoporous silica spheres employed during this study is primarily based on a procedure reported by Kim *et al.* (2004). This synthesis procedure was refined to achieve the specific material structure required for the applications shown in this study. The synthesis refinement incorporated assessing the impact of reactant alteration during the materials' production, including molecular template and parameter adjustment. The resultant materials were then analysed by microscopy, nitrogen physisorption and X-ray techniques to distinguish the most promising materials. An increase in surfactant and ageing temperature was shown to result in the best material candidate on which to focus application studies.

Once a basic and successful synthesis procedure was in operation, work was directed towards surface engineering of the mesoporous silica spheres to allow absorption applications of different molecules. Developing a procedure for successful surface chemical modification was another focus in this work. After application of different alteration techniques, the resultant functionalised materials were characterised using elemental analysis, nitrogen physisorption, X-ray diffraction, microscopy and infrared techniques. A facile refluxing procedure was emphasised as the best process to form optimum mono-functionalised and bi-functionalised mesoporous spheres as it retained spherical morphology and pore structure to allow absorption systems to be expanded.

The materials group at UCC is primarily focused on applying mesoporous materials in catalysis and electronics. The application studies in this work expand this research to environmental and analytical areas. This may provide a basis for future commercial exploitation through sales or licensing.

Increased pollution problems within the environment highlight the research needed for ecological clean-up. The environmental application studied in this study incorporates remediation of pollutants, specifically metal ions and nanoparticles. The metal ion and nanoparticle extraction was achieved by filtration of polluted samples through a fixed bed of absorbents. Atomic absorption and UV-Vis techniques were used to quantify the removal of metal ions and nanoparticles from solution. The applied absorbents included mono-functionalised and bi-functionalised mesoporous silica spheres. The mono-functionalised absorbents were chemically modified using either an aminopropyl or a mercaptopropyl ligand, whereas the bi-functionalised absorbent was modified with both an aminopropyl and mercaptopropyl ligand. Each mono-functionalised absorbent showed attraction to particular metal ions as expected, while the bi-functionalised absorbent removed a mix of metal ions. These completed experiments emphasise the suitability of mesoporous silica spheres for metal pollutant remediation. An industrial sample supplied by the EPA was also filtered through the fixed bed of absorbents. The successful extraction of metal ions from this industrial sample shows that the absorbent materials are suitable for waste-water clean-up in industry.

The results of this study emphasise and support the idea that mesoporous silica materials can be tailored to specific applications. The relationship shown between material science and environmental science highlights that the remediation of pollutants from ecological systems could represent a new future direction in which nanomaterial research should be guided. Overall the results confirm that synthesised mesoporous material could be successfully applied for waste-water treatment in industry.

References

Ahrland, S., Chatt, J. *et al.*, 1958. The relative affinities of ligand atoms for acceptor molecules and ions. *Quarterly Review of the Chemistry Society* **12:** 265.

Ajay, K.M., Mishraa, G.K., Raia, P.K., Rajagopala, C. and Nagarb, P.N., 2005. Removal of heavy metal ions from aqueous solutions using carbon aerogel as an adsorbent. *Journal of Hazardous Materials* **122(1–2):** 161–170.

Ali, I. and Aboul-Enein, H.Y., 2006. *Instrumental Methods in Metal Ion Speciation*. Taylor & Francis Group, Oxford, UK.

Armstrong, B., Hutchinson, E. *et al.*, 2004. Lung cancer risk exposure to polycyclic aromatic hydrocarbons: a review and meta-analysis. *Environmental Health Perspectives* **112:** 970–978.

Avakian, M.D., Dellinger, B. *et al.*, 2002. Environmentally persistent free radicals amplify ultrafine particle mediated cellular oxidative stress and cytotoxicity. *Environmental Health Perspectives* **110:** 1155–1162.

Avantaggiato, G., Havenaar, R. *et al.*, 2004. Evaluation of the intestinal absorption of deoxynivalenol and nivalenol by an in vitro gastrointestinal model, and the binding efficacy of activated carbon and other adsorbent materials. *Food and Chemical Toxicology* **42:** 817–824.

Becheri, A., Durr, M. *et al.*, 2008. Synthesis and characterization of zinc oxide nanoparticles: applications to textiles as UV-absorbers. *Journal of Nanoparticle Research* **10(4):** 679–689.

Beck, J.S., Vartulli, J.C. *et al.*, 1992. A new family of mesoporous molecular sieves prepared with liquid crystal templates. *Journal of American Chemistry Society* **114:** 10834–10843.

Bingau, P., Lonsdale, H. *et al.*, 1986. *Synthetic Membranes: Science, Engineering and Application*. Reidel Publishing Company, Dordrecht, Holland.

Blin, J.L., Otjacques, C. *et al.*, 2000. Pore size engineering of mesoporous silicas using decane as expander. *Langmuir* **16**(**9):** 4229–4236.

Blin, J.L. and Su, B.L., 2002. Tailoring pore size of ordered mesoporous silicas using one or two organic auxiliaries as expanders. *Langmuir* **18**(**13):** 5303–5308.

Bois, L., Bonhomme, A. *et al.*, 2002. Functionalised silica for heavy metal ions adsorption. *Colloids and Surfaces A: Physiochemical and Engineering Aspects* **221(1–3):** 221–230.

Carro, A. and Mejuto, M., 2000. Application of chromatographic and electrophoretic methodology to the speciation of organomercury compounds in food analysis. *Journal of Chromatography A* **882:** 283–307.

Celik, A. and Demirba, A., 2005. Removal of heavy metal ions from aqueous solutions via adsorption onto modified lignin from pulping wastes. *Energy Sources* **27:** 1167–1177.

Coleman, N.R.B., Morris, M.A. *et al.*, 2001a. The formation of dimensionally ordered silicon nanowires within mesoporous silica. *Journal of American Chemistry Society* **123:** 187–188.

Coleman, N.R.B., O' Sullivan, N. *et al.*, 2001b. Synthesis and characterization of dimensionally ordered semiconductor nanowires within mesoporous silica. *Journal of American Chemistry Society* **123:** 7010–7016.

Coleman, N.R.B., Ryan, K.M. *et al.*, 2001c. The formation of dimensionally ordered germanium nanowires within mesoporous silica. *Chemical Physics Letters* **343:** 1–6.

Copley, M., 2006. *Syntheses, Modification and Application of Hexagonally Ordered Mesoporous Silica*. PhD Thesis, University College Cork, Cork, Ireland.

Cotton, F.A. and Wilkinson, G., 1966. *Advanced Inorganic Chemistry*. Wiley & Sons.

Crowley, T.A., Ziegler, K.J. *et al.*, 2003. Synthesis of metal and metal oxide nanowire and nanotube arrays within a mesoporous silica template. *Chemical Materials* **15:** 3518–3522.

Darbandi, M., Lu, W. *et al.*, 2006. Silica encapsulation of hydrophobically ligated PBSE nanocrystals. *Langmuir* **22:** 4371–4375.

Dunnick, J., Elwell, M. *et al.*, 1995. Comparative carcinogenic effects of nickel subsulfide, nickel oxide or nickel sulfate hexahydrate chronic exposure in the lung. *Cancer Research* **55(22):** 5251–5256.

Ekmekyapara, F., Aslanb, A. *et al.*, 2006. Biosorption of copper(II) by nonliving lichen biomass of *Cladonia rangiformis* hoffm. *Journal of Hazardous Materials* **137(1):** 293–298.

EPA, 2004. *European Communities (Drinking Water) Regulations*. Environmental Protection Agency, Johnstown Castle Estate, Wexford, Ireland.

EPA, 2006. *Environment in Focus 2006*. Environmental Protection Agency, Johnstown Castle Estate, Wexford, Ireland.

EPA, 2007. *Nanotechnology White Paper US Environmental Protection Agency Report.* US Environmental Protection Agency, Washington, DC, USA.

Esmat, A.A., 1993. Damage to plants due to industrial pollution and their use as bioindicators in Egypt. *Environmental Pollution* **81(3):** 251.

Estermann, M., McClusker, L.B. *et al.*, 1991. A synthetic gallophosphate molecular sieve with a 20-tetrahedral-atom pore opening. *Nature* **353:** 320–323.

Flodstrom, K. and Alfresson, V., 2003. Influence of the block length of triblock copolymers on the formation of mesoporous silica. *Microporous and Mesoporous Materials* **59(2):** 167–176.

Fryxell, G.E., Feng, X. *et al.*, 1997. Functionalised monolayers on ordered mesoporous supports. *Science* **276(5314):** 923–926.

Fukuoka, A., Araki, H. *et al.*, 2002. Template synthesis of nanoparticle arrays of gold and platinum in mesoporous silica films. *Nano Letters* **2:** 793–795.

Gallis, K.W., Araujo, J.T. *et al.*, 1999. The use of mesoporous silica in liquid chromatography. *Advanced Materials* **11(17):** 1452–1455.

Gojova, A., Guo, B. *et al.*, 2007. Zinc oxide nanoparticles. *Environmental Health Perspectives* **115(3):** 403–409.

Han, S., Xu, J. *et al.*, 2004. Synthesis of high-quality MCM-48 mesoporous silica using gemini surfactant dimethylene-1,2-bis(dodecyldimethylammonium bromide. *Journal of Physical Chemistry B* **108:** 15043–15048.

Hanrahan, J.P., Copley, M.P. *et al.*, 2004. Pore expansion in mesoporous silicas using supercritical carbon dioxide. *Chemistry of Materials* **16(3):** 424–427.

Hayes, A.W. and Holland, M.G., 2001. Principles and methods of toxicology. *Int J Med Toxicol* **4(5):** 41.

Healy, L.O., Owens, V.P. *et al.*, 2003. Supercritical fluid generated stationary phases for liquid chromatography and capillary electrochromatography. *Analytical Chemistry* **75:** 5860–5869.

Hempel, M., Chau, Y. *et al.*, 1995. Toxicity of organmercury compounds: bioassay results as a basis for risk assessment. *Analyst* **120:** 721.

Hu, J.-D., Li, Y.-X. *et al.*, 2007. Preparation and characterization of ceria nanoparticles using crystalline hydrate cerium propionate as precursor. *Materials Letters* **61:** 4989–4992.

Huo, Q., Margolese, D.I. *et al.*, 1996. Surfactant control of phases in the synthesis of mesoporous silica-based materials. *Chemical Materials* **8:** 1147.

IARC, 1989. *Chromium, Nickel and Welding*. International Agency for Research on Cancer, Lyon, France.

Irving, H. and Williams, R.J.P., 1953. Stability constants of 2-mercaptohistamine metal complexes. *Journal of the American Chemical Society* 3192–3210.

IUPAC, 1976. Manual of Symbols and Terminology for Physiochemical Quantities and Units-Appendix II. *Pure and Applied Chemistry* **46:** 71–90.

Jaimez, J., Fente, C.A. *et al.*, 2000. Application of the assay of aflatoxins by liquid chromatography with fluorescence detection in food analysis. *Journal of Chromatography A* **882:** 1–10.

Kang, T., Park, Y. *et al.*, 2004. Highly selective adsorption of Pt^{2+} and Pd^{2+} using thiol-functionalized mesoporous silica. *Industrial Engineering Chemistry & Research* **43:** 1478–1484.

Kasprzak, K., Sunderman Jr, F.S. *et al.*, 2003. Nickel carcinogenesis. *Mutation Research* **533(1–2):** 67–97.

Kiffs, R.J., 1987. General inorganic effluents. General inorganic effluents. *In:* Barnes, D., Forster, C.F. and Hrudey, S.E. (Eds), *Surveys in Industrial Wastewater Treatment—Manufacturing and Chemical Industries.* Vol. 3, Longman, New York, NY, USA.

Kim, T.-W., Ryoo, R. *et al.*, 2004. Tailoring the pore structure of SBA-16 silica molecular sieve through the use of coploymer blends and control of synthesis temperature and time. *Journal of Physical Chemistry B* **108(31):** 11480–11489.

Kipkemboi, P., Fogden, A. *et al.*, 2001. Triblock copolymers as templates in mesoporous silica formation: Structural dependence on polymer chain length and synthesis temperature. *Langmuir* **17:** 5398–5402.

Kresge, C.T., Leonwicz, M.E. *et al.*, 1992. Ordered mesoporous molecular sieves synthesized by a liquid crystal template mechanism. *Nature* **359:** 710.

Kruk, M., Jaroniec, M. *et al.*, 1997. Application of large pore MCM-41 molecular sieves to improve pore size analysis using nitrogen adsorption measurements. *Langmuir* **13:** 6267.

Kruk, M., Jaroniec, M. *et al.*, 2000. New insights into pore-size expansion of mesoporous silicates using long-chain amines. *Microporous and Mesoporous Materials* **35:** 545–553.

Lindman, S., Lynch, I. *et al.*, 2006. Systematic investigation of the thermodynamics of HSA adsorption to N-*iso*-propylacrylamide/N-*tert*-butylacrylamide copolymer nanoparticles. Effects of particle size and hydrophobicity. *Nano Letters* **7(4):** 914–920.

Linssen, T., Cassiers, K. *et al.*, 2003. Mesoporous templated silicates. *Advanced Colloids Interface Science* **103:** 121–147.

Liu, H., Zhang, L. *et al.*, 1993. Analysis of sorption hysteresis in mesoporous solids using a pore network model. *Journal of Colloid Interface Science* **156:** 285.

Lundqvist, M., Sethson, I. *et al.*, 2004. Protein adsorption onto silica nanoparticles: Conformational changes depend on the particles curvature and the protein stability. *Langmuir* **20(24):** 10639–10647.

Lundqvist, M., Sethson, I. *et al.*, 2005. High-resolution 2D H-N NMR characterization of persistent structural alterations of proteins induced by interactions with silica nanoparticles. *Langmuir* **21(13):** 5974–5979.

Lyon, D.Y., Adams, L.K. *et al.*, 2006. Antibacterial activity of fullerene water suspensions: Effects of preparation method and particle size *Environmental Science Technology* **40:** 4360–4366.

Ma, Y., Qi, L. *et al.*, 2003. Large-pore mesoporous silica spheres: synthesis and application in HPLC. *Colloids and Surfaces A: Physicochemical and Engineering Aspects* **229:** 1–8.

Madler, L., Stark, W.J. *et al.*, 2002. Simultaneous deposition of gold nanoparticles during flame synthesis of titania and silica. *Journal of Materials Research* **17:** 1356–1362.

Malvern, 2007. *Properties and Current Applications of Nanoparticles*. Worcestershire, UK.

Maynard, A., 2006. *Nanotechnology: A Research Strategy for Addressing Risk*. Available online at http://www.nanotechproject.org.

Meena, A.K., Mishra, G.K. *et al.*, 2005. Removal of heavy metal ions from aqueous solutions using carbon aerogel as an adsorbent. *Journal of Hazardous Materials* **122(1–2):** 161–170.

Mehdi, A., Dourdain, S. *et al.*, 2006. First direct synthesis of highly ordered bi-functionalized mesoporous silica thin films. *Journal of Nanoscience and Nanotechnology* **6:** 377–381.

Mercier, L. and Pinnavaia T., 1998. Heavy Metal ion adsorbents formed by the grafting of a thiol functionality to mesoporous silica molecular sieves: factors affecting Hg(II) uptake. *American Chemical Society* **32(18):** 2749–2754.

Morawska, L. and Zhang, J., 2002. Combustion sources of particles: health relevance and source signatures. *Chemosphere* **49(9):** 1045–1058.

Murray, P.G., 2004. Nanoparticle dispersions for polishing applications. *Nanotechnology* **3:** 387–390.

Namasivayam, C. and Ranganathan, K., 1995. Removal of Pb(II), Cd(II), Mi(II) and mixture of metal ions by adsorption on waste Fe(III)/Cr(III) hydroxide and fixed bed studies. *Environmental Technology* **16:** 851–860.

Nestle, O., Speidel, H. *et al.*, 2002. High nickel release from 1 and 2 euro coins. *Nature* **419(132)**.

Nogawa, K. *et al.*, 2004. Environmental cadmium exposure, adverse effects, and preventative measures in Japan. *Biometals* **17(5):** 581–7.

Northcott, K., Kokusen, H. *et al.*, 2006. Synthesis and surface modification of esoporous silica SBA-15 for the adsorption of metal ions. *Separation Science and Technology* **41:** 1829–1840.

Nowack, B. and Bucheli, T.D., 2007. Occurrence, behavior and effects of nanoparticles in the environment. *Environmental Pollution* **150:** 5–22.

Nriagu, J., 1989. A global assessment of natural sources of atmospheric trace metals. *Nature* **338:** 47.

NTP (National Toxicology Program), 2008. *11th Report on Carcinogens*. US Department of Health and Human Services, Washington, USA.

O'Neil, A.S., Mokaya, R. *et al.*, 2002. Supercritical fluid-mediated alumination of mesoporous silica and its beneficial effect on hydrothermal stability. *Journal of American Chemistry Society* **124:** 10636–10637.

Oberdorster, G., Oberdorster, E. *et al.*, 2004. Nanotoxicology: An emerging discipline evolving from studies of ultrafine particles. *Environmental Health Perspectives* **112:** 1058–1062.

Park, B.-G., Guo, W. *et al.*, 2003. Preparation and characterization of organo-modified SBA-15 by using polypropylene glycol as a swelling agent. *Microporous and Mesoporous Materials* **66(2):** 229–238.

Pearson, R.G., 1963. Hard and soft acids and bases. *Journal of the American Chemical Society* **85(22):** 3533.

Pursch, M., Brindle, R. *et al.*, 1997. Stationary interphases with extended alkyl chains: A comparative study on chain order by solid-state NMR spectroscopy. *Solid State Nuclear Magnetic Resonance* **9:** 191–201.

Roach, P., Farrar, D. *et al.*, 2006. Surface tailoring for controlled protein adsorption: Effect of topography at the nanometer scale and chemistry. *Journal of American Chemistry Society* **128(12):** 3939–3945.

Rothen-Rutishauser, B.M., Schurch, S. *et al.*, 2006. Interaction of fine particles and nanoparticles with red blood cells visualized with advanced microscopic techniques. *Environmental Science Technology* **40:** 4353–4359.

Ryan, K.M., Coleman, N.R.B. *et al.*, 2002. Control of pore morphology in mesoporous silicas synthesised from triblock copolymer templates. *Langmuir* **18:** 4996–5001.

Ryan, K.M., Erts, D. *et al.*, 2003. Three dimensional architectures of ultra-high density semiconducting nanowires deposited on chip. *Journal of American Chemistry Society* **125:** 6284–6288.

Say, R., Birlik, E. *et al.*, 2006. Removal of heavy metal ions by dithiocarbamate-anchored polymer/organosmectite composites. *Applied Clay Science* **31:** 298–305.

Selvam, P., Bhatia, S.K. *et al.*, 2001. Recent advances in processing and characterization of periodic mesoporous MCM-41 silicate molecular sieves. *Industrial Engineering Chemistry & Research* **40(15):** 3237–3261.

Sing, K.S., Everett, D.H. *et al.*, 1985. Reporting physisorption data for gas/solid systems with special reference to the determination of surface area and porosity. *Pure Applied Chemistry* **57:** 603.

Smart, S.K., Cassady, A.I. *et al.*, 2006. The biocompatibility of carbon nanotubes. *Carbon* **44(6):** 1034–1047.

Socrates, G., 1994. Infrared characteristic group frequencies: Tables and charts. *Journal of Molecular Structure* **372(2–3):** 285.

Stoeppler, M., 1992. *Hazardous Metals in the Environment*. Elsevier.

Stohs, S. and Bagchi, D., 1995. Oxidative mechanisms in the toxicity of metal ions. *Free Radical Biology and Medicine* **18:** 321–336.

Unob, F., Wongsiri, B. *et al.*, 2007. Reuse of waste silica as adsorbent for metal removal by iron oxide modification. *Journal of Hazardous Materials* **142(1–2):** 455.

Uysal, M. and Ar, I., 2007. Removal of Cr (VI) from industrial wastewater by adsorption Part 1: Determination of optimum conditions. *Journal of Hazardous Materials* **149(2):** 482–491.

Webb, P.A. and Orr, C., 1997. *Analytical Methods in Fine Particle Technology*. Micromeritics Instrument Corporation. Norcross, GA, USA.

Wu, C.G. and Bein, T., 1994. Conducting carbon wires in ordered, nanometer-sized channels. *Science* **266(5187):** 1013–1015.

Xing, R. and Rankin, S.E., 2008. Reactive pore expansion during ammonia vapor post-treatment of ordered mesoporous silica prepared with mixed glucopyranoside and cationic surfactants. *Microporous and Mesoporous Materials* **108(1):** 65–76.

Yamada, T., Zhou, H. *et al.*, 2002. Pore size controlled mesoporous silicate powder prepared by triblock copolymer templates. *Materials Letters* **56:** 93–96.

Yang, M., Jensen, L.T., Gardner, A.J. and Culotta, V.C., 2005. Manganese toxicity and *Saccharomyces cerevisiae* Mam3p, a member of the ACDP (ancient conserved domain protein) family. *Biochemical Journal* **386:** 479–487.

Yurong, M., Limin, Q. *et al.*, 2003. Large pore mesoporous silica spheres synthesis and application in HPLC. *Colloids and Surfaces A: Physicochemical and Engineering Aspects.* **229(1):** 1–8.

Zhang, W.-H., Lu, X.-B. *et al.*, 2004. Synthesis and characterization of bifunctionalized ordered mesoporous materials. *Advanced Functional Materials* **14:** 544.

Zhang, Y., Yang, H. *et al.*, 2007. Synthesis of an affinity adsorbent based on silica gel and its application in

endotoxin removal. *Reactive and Functional Polymers* **67:** 728–736.

Zhao, D., Huo, Q. *et al.*, 1998. Nonionic triblock and star diblock copolymer and oligomeric surfactant syntheses of highly ordered, hydrothermally stable, mesoporous silica structures. *Journal of American Chemistry Society* **120(24):** 6024–6036.

Zhao, X.S., Lu, G.Q.M. and Millar, G.J.,1996. Advances in mesoporous molecular sieve MCM-41. *Industrial & Engineering Chemistry Research* **35:** 2075–2090.

Zhu, G., Yang, Q. *et al.*, 2005. Synthesis of bifunctionalised mesoporous organosilica spheres for high performance liquid chromatography. *Journal of Chromatography A* **1103:** 257–264.

An Ghníomhaireacht um Chaomhnú Comhshaoil

Is í an Gníomhaireacht um Chaomhnú Comhshaoil (EPA) comhlachta reachtúil a chosnaíonn an comhshaol do mhuintir na tíre go léir. Rialaímid agus déanaimid maoirsiú ar ghníomhaíochtaí a d'fhéadfadh truailliú a chruthú murach sin. Cinntímid go bhfuil eolas cruinn ann ar threochtaí comhshaoil ionas go nglactar aon chéim is gá. Is iad na príomh-nithe a bhfuilimid gníomhach leo ná comhshaol na hÉireann a chosaint agus cinntiú go bhfuil forbairt inbhuanaithe.

Is comhlacht poiblí neamhspleách í an Ghníomhaireacht um Chaomhnú Comhshaoil (EPA) a bunaíodh i mí Iúil 1993 faoin Acht fán nGníomhaireacht um Chaomhnú Comhshaoil 1992. Ó thaobh an Rialtais, is í an Roinn Comhshaoil agus Rialtais Áitiúil a dhéanann urraíocht uirthi.

ÁR bhFREAGRACHTAÍ

CEADÚNÚ

Bíonn ceadúnais á n-eisiúint againn i gcomhair na nithe seo a leanas chun a chinntiú nach mbíonn astuithe uathu ag cur sláinte an phobail ná an comhshaol i mbaol:

- áiseanna dramhaíola (m.sh., líonadh talún, loisceoirí, stáisiúin aistrithe dramhaíola);
- gníomhaíochtaí tionsclaíocha ar scála mór (m.sh., déantúsaíocht cógaisíochta, déantúsaíocht stroighne, stáisiúin chumhachta);
- diantalmhaíocht;
- úsáid faoi shrian agus scaoileadh smachtaithe Orgánach Géinathraithe (GMO);
- mór-áiseanna stórais peitreail.
- Scardadh dramhuisce

FEIDHMIÚ COMHSHAOIL NÁISIÚNTA

- Stiúradh os cionn 2,000 iniúchadh agus cigireacht de áiseanna a fuair ceadúnas ón nGníomhaireacht gach bliain.
- Maoirsiú freagrachtaí cosanta comhshaoil údarás áitiúla thar sé earnáil - aer, fuaim, dramhaíl, dramhuisce agus caighdeán uisce.
- Obair le húdaráis áitiúla agus leis na Gardaí chun stop a chur le gníomhaíocht mhídhleathach dramhaíola trí comhordú a dhéanamh ar líonra forfheidhmithe náisiúnta, díriú isteach ar chiontóirí, stiúradh fiosrúcháin agus maoirsiú leigheas na bhfadhbanna.
- An dlí a chur orthu siúd a bhriseann dlí comhshaoil agus a dhéanann dochar don chomhshaol mar thoradh ar a ngníomhaíochtaí.

MONATÓIREACHT, ANAILÍS AGUS TUAIRISCIÚ AR AN GCOMHSHAOL

- Monatóireacht ar chaighdeán aeir agus caighdeáin aibhneacha, locha, uiscí taoide agus uiscí talaimh; leibhéil agus sruth aibhneacha a thomhas.
- Tuairisciú neamhspleách chun cabhrú le rialtais náisiúnta agus áitiúla cinntí a dhéanamh.

RIALÚ ASTUITHE GÁIS CEAPTHA TEASA NA HÉIREANN

- Cainníochtú astuithe gáis ceaptha teasa na hÉireann i gcomhthéacs ár dtiomantas Kyoto.
- Cur i bhfeidhm na Treorach um Thrádáil Astuithe, a bhfuil baint aige le hos cionn 100 cuideachta atá ina mór-ghineadóirí dé-ocsaíd charbóin in Éirinn.

TAIGHDE AGUS FORBAIRT COMHSHAOIL

- Taighde ar shaincheisteanna comhshaoil a chomhordú (cosúil le caighdéan aeir agus uisce, athrú aeráide, bithéagsúlacht, teicneolaíochtaí comhshaoil).

MEASÚNÚ STRAITÉISEACH COMHSHAOIL

- Ag déanamh measúnú ar thionchar phleananna agus chláracha ar chomhshaol na hÉireann (cosúil le pleananna bainistíochta dramhaíola agus forbartha).

PLEANÁIL, OIDEACHAS AGUS TREOIR CHOMHSHAOIL

- Treoir a thabhairt don phobal agus do thionscal ar cheisteanna comhshaoil éagsúla (m.sh., iarratais ar cheadúnais, seachaint dramhaíola agus rialacháin chomhshaoil).
- Eolas níos fearr ar an gcomhshaol a scaipeadh (trí cláracha teilifíse comhshaoil agus pacáistí acmhainne do bhunscoileanna agus do mheánscoileanna).

BAINISTÍOCHT DRAMHAÍOLA FHORGHNÍOMHACH

- Cur chun cinn seachaint agus laghdú dramhaíola trí chomhordú An Chláir Náisiúnta um Chosc Dramhaíola, lena n-áirítear cur i bhfeidhm na dTionscnamh Freagrachta Táirgeoirí.
- Cur i bhfeidhm Rialachán ar nós na treoracha maidir le Trealamh Leictreach agus Leictreonach Caite agus le Srianadh Substaintí Guaiseacha agus substaintí a dhéanann ídiú ar an gcrios ózóin.
- Plean Náisiúnta Bainistíochta um Dramhaíl Ghuaiseach a fhorbairt chun dramhaíl ghuaiseach a sheachaint agus a bhainistiú.

STRUCHTÚR NA GNÍOMHAIREACHTA

Bunaíodh an Ghníomhaireacht i 1993 chun comhshaol na hÉireann a chosaint. Tá an eagraíocht á bhainistiú ag Bord lánaimseartha, ar a bhfuil Príomhstiúrthóir agus ceithre Stiúrthóir.

Tá obair na Gníomhaireachta ar siúl trí ceithre Oifig:

- An Oifig Aeráide, Ceadúnaithe agus Úsáide Acmhainní
- An Oifig um Fhorfheidhmiúchán Comhshaoil
- An Oifig um Measúnacht Comhshaoil
- An Oifig Cumarsáide agus Seirbhísí Corparáide

Tá Coiste Comhairleach ag an nGníomhaireacht le cabhrú léi. Tá dáréag ball air agus tagann siad le chéile cúpla uair in aghaidh na bliana le plé a dhéanamh ar cheisteanna ar ábhar imní iad agus le comhairle a thabhairt don Bhord.

NDP
National Development Plan 2007 - 2013

Science, Technology, Research and Innovation for the Environment (STRIVE) 2007-2013

The Science, Technology, Research and Innovation for the Environment (STRIVE) programme covers the period 2007 to 2013.

The programme comprises three key measures: Sustainable Development, Cleaner Production and Environmental Technologies, and A Healthy Environment; together with two supporting measures: EPA Environmental Research Centre (ERC) and Capacity & Capability Building. The seven principal thematic areas for the programme are Climate Change; Waste, Resource Management and Chemicals; Water Quality and the Aquatic Environment; Air Quality, Atmospheric Deposition and Noise; Impacts on Biodiversity; Soils and Land-use; and Socio-economic Considerations. In addition, other emerging issues will be addressed as the need arises.

The funding for the programme (approximately €100 million) comes from the Environmental Research Sub-Programme of the National Development Plan (NDP), the Inter-Departmental Committee for the Strategy for Science, Technology and Innovation (IDC-SSTI); and EPA core funding and co-funding by economic sectors.

The EPA has a statutory role to co-ordinate environmental research in Ireland and is organising and administering the STRIVE programme on behalf of the Department of the Environment, Heritage and Local Government.

epa
Environmental Protection Agency
An Ghníomhaireacht um Chaomhnú Comhshaoil

ENVIRONMENTAL PROTECTION AGENCY
PO Box 3000, Johnstown Castle Estate, Co. Wexford, Ireland
t 053 916 0600 f 053 916 0699
LoCall 1890 33 55 99
e info@epa.ie w http://www.epa.ie

SSTI
Strategy for Science, Technology and Innovation

Comhshaol, Oidhreacht agus Rialtas Áitiúil
Environment, Heritage and Local Government